Catalytic Hydrocracking of Bibenzyl

Reaction Temp. = 350°C, Reaction Time = 3 hrs, Sulfur = 0.10 g, H_2 = 1000 psig			
Catalyst (wt.%)	Conversion (%)	Benzene (mmol)	Ethylbenzene (mmol)
Fe_3APC (10)	84	1.79	0.57
Fe_3APC (10)	98	2.26	0.93
Fe_3ZPC (10)	67	1.28	0.34
K-10Fe_3 (10)	65	1.38	0.40
IMont (10)	61	1.12	0.46
Magnetite (10)	3	Trace	
Maghemite (10)	5	Trace	
K-10Fe_2O_3 (10)	57	2.40	0.26

Hydrogenation Activity of Iron Catalysts

H_2 = 1000 psig, S = 0.03 g				
Catalyst (wt.%)	Susbstrate (mmol)	Temp. (°C)	Conv. (%)	Cracked Products (%)
None	Pyrene	400	6	0
IAPC (50)	Pyrene	400	67	36
IAPC (50)	Pyrene	440	50	47
Fe_3APC (10)	Pyrene	350	76	17
IMont (50)	Pyrene	400	68	25
NiMoCrPC (50)	Pyrene	400	64	36

Hydrogenation Activity of Iron Catalysts

H_2 = 1000 psig, S = 0.03 g				
Catalyst (wt.%)	Susbstrate (mmol)	Temp. (°C)	Conv. (%)	Cracked Products (%)
IAPC (50)	1-Methyl naphthalene	300	87	27
IMont (50)	1-Methyl naphthalene	300	82	23
IAPC (50)	Diphenyl Ether	400	76	99
IAPC (50)	Phenol	400	60	-

Catalytic Liquefaction with Clay-Supported Iron Sulfides

Reaction Temp. = 425°C, Reaction Time = 1 hr,
H_2 = 1000 psi (cold)
Coal/tetralin = 0.5, Catalysts = 10 wt%

Coal (g)	Catalyst (wt. %)	Sulfur (g)	Conv. (%)	Heptane-I (%)	Heptane-S (%)
ARW (7.0)	None	None	89	41	48
IEW (5.3)	None	None	86	40	47
ARW (7.0)	Fe_3APC (10)	None	87	54	33
ARW (7.0)	Fe_3APC (10)	0.10	91	38	53
IEW (5.34)	Fe_3APC (10)	0.10	95	41	54
IEW (5.41)	K10Fe_3 (10)	0.10	92	35	57
ARW (7.0)	IMont (10)	0.10	93	26	67
IEW (5.37)	IMont (10)	0.10	95	26	69

ARW = as received Wyodak
IEW = 7.0 g AR coal was acid-washed and dried

Catalytic Liquefaction with Clay-Supported Iron Sulfides

Blind Canyon (Argonne Premium Sample)

Reaction Temp. = 425°C, Reaction Time = 1 hr, H_2 = 1000 psi (cold) Coal/tetralin = 0.5, Catalysts = 10 wt%				
Catalyst (wt. %)	Sulfur (g)	Conv. (%)	Heptane-I (%)	Heptane-S (%)
None	None	91	58	33
Fe_3APC (10)	None	93	61	32
Fe_3APC (10)	0.10	92	55	37

Catalytic Liquefaction of LSW Intermediate

Temperature = 425°C, H_2 = 1000 psi, LSW/Tetralin = 0.5, S = 0.01g				
Catalyst (wt. %)	**Time (hr)**	**THF-I**	**Heptane-I**	**Heptane-S**
None	1	0	85	15
Fe_3-APC (10)	1	0	70	30
Fe_3-APC (10)	3	0	58	42
IMont (10)	1	0	55	45
Co-Moly (10)	1	0	49	51

Title: ACTIVITY TESTING OF FINE-PARTICLE SIZE, IRON CATALYSTS FOR COAL LIQUEFACTION

Authors: Frances V. Stohl, Kathleen V. Diegert, Thomas P. Gugliotta

Organization: Sandia National Laboratories, Albuquerque, NM 87185

Contract No.: DE-AC04-76DP00789

Period of Performance: January 1992 -

Objectives: To evaluate and compare the activities/selectivities of fine-particle size catalysts being developed in the DOE/PETC Advanced Research (AR) Coal Liquefaction program by using standard coal liquefaction activity test procedures.

Accomplishments: The use of fine-particle size (<40 nm) unsupported catalysts in direct coal liquefaction may result in improved economics due to possible enhanced yields of desired products, the potential for decreasing reaction severity, and the possibility of using less catalyst. Sandia has developed a standard testing procedure for evaluating and comparing the many different fine-particle catalysts being developed in DOE's AR Program. The test procedure uses phenanthrene as the reaction solvent, the DECS-17 Blind Canyon Coal, and a statistical experimental design to enable evaluation of the catalysts over ranges of temperature (350 to 400°C), time (20 to 60 minutes), and catalyst loading (0 to 1 wt% on a dmmf coal basis). Testing is performed in batch microautoclave reactors with continuous monitoring of reaction temperature and pressure. Product analyses include tetrahydrofuran (THF) conversion, heptane conversion, solvent recovery, and gas analyses. Experiments showed that using phenanthrene as the solvent in the testing procedure yielded significant differences between thermal and catalytic reactions, whereas using a good hydrogen donor such as 9,10-dihydrophenanthrene (DHP) showed no catalytic effects. The testing procedure with phenanthrene has been used to evaluate catalytic effects of a standard catalyst (-100 mesh pyrite) and the University of Pittsburgh's sulfated iron oxide catalyst.

Plans: Future work will include testing additional catalysts being developed in the AR Coal Liquefaction Program, characterizing reaction products, and evaluating the best catalyst using an expanded experimental design.

Project Team: Frances Stohl, Kathleen Diegert, Thomas Gugliotta, Carlos Quintana, Elaine Boespflug

Introduction

There are several potential advantages of using cheap, unsupported, fine-particle size (<40 nm) catalysts in direct coal liquefaction. These include improved coal/catalyst contact due to good dispersion[1] of the catalyst, and the potential for using low quantities of catalyst (≤0.5% based on the weight of coal) because of their very high surface areas. These catalysts could be combined with the coal as either active catalysts or catalyst precursors that would be activated in situ. Research efforts that have been performed to develop fine-particle size, unsupported catalysts for direct coal liquefaction[2] indicate that the use of these catalysts could result in significant process improvements, such as enhanced yields of desired products, less usage of supported catalyst, and possibly lower reaction severities. These improvements would result in decreased costs for coal liquefaction products.

The Advanced Research (AR) Coal Liquefaction Program, which is managed by the United States Department of Energy's Pittsburgh Energy Technology Center (PETC), is funding numerous research efforts aimed at developing these types of catalysts for direct liquefaction. Although most catalyst developers have the capability of testing the performances of the catalysts they develop, it is difficult if not impossible to compare results among researchers because of the different testing procedures used. Some of the differences include reactors, reaction temperatures, reaction times, pressures, hydrogen donor solvents, solvent to coal ratios, and workup procedures. Therefore, to guide the research and development efforts for these fine-particle size, unsupported catalysts, it is necessary to evaluate each catalyst's performance under standard test conditions so that the effects of catalyst formulations from different laboratories can be compared.

The objectives of this project are to develop standard coal liquefaction test procedures and to perform the testing of the novel fine-particle size liquefaction catalysts being developed in the PETC AR Coal Liquefaction program. Previously reported work[(3)] defined the factorial experimental design to be used in this project and described results of the initial evaluation of the test procedures and experimental design by using 9,10-dihydrophenanthrene (DHP) as the reaction solvent and commercially available pyrite as the catalyst. These results indicated that the standard test procedures were good, although catalytic effects were not observed. To be able to compare the many different catalysts being developed in DOE/PETC's AR program, it is desirable to have large differences between catalytic and thermal reactions. This paper will describe results that led to development of an improved standard test procedure by changing the reaction solvent. Results obtained using this revised standard test with pyrite and with the University of Pittsburgh's sulfated iron oxide catalyst will also be reported.

Experimental Section

Materials. The coal being used in this project is the DECS-17 Blind Canyon Coal obtained from The Penn State Coal Sample Bank. It is a HVA bituminous coal with 0.36% iron, 0.02% pyritic sulfur, and 7.34% mineral matter (on a dry basis). The particle size is -60 mesh. 9,10-dihydrophenanthrene (DHP) and phenanthrene were evaluated as reaction solvents for use in the standard test. Pyrite (99.9% pure on a metals basis) with a -100 mesh particle size was

obtained from Johnson-Matthey. The sulfated iron oxide catalyst was obtained from the University of Pittsburgh.

Microautoclave Reactors. The testing is performed using batch microautoclaves made of type 316 stainless steel components. The total volume of a reactor is 43 cm^3 with a liquid capacity of 8 cm^3. The reactors are loaded with 1.67g coal and 3.34g reaction solvent. If the reaction is catalytic, the catalyst loading will be either 0.5 wt% or 1.0 wt% on an as-received coal basis. The reactors are charged to 800 psig H_2 (cold charge) and heated to reaction temperatures in fluidized-sand baths. Temperatures, pressures and times are recorded with a digital data acquisition system every 30 seconds during the course of the reactions. Following the heating period, the reactors are rapidly quenched to ambient temperature in a water bath and a gas sample is collected. The reaction data is analyzed to determine the actual reaction time and the averages and standard deviations for reaction temperature and pressure. Heat up times and quench times are also determined.

Product Workup Procedures. The reaction products are rinsed out of the reactors with THF. THF and heptane solvent solubilities are measured using a Millipore 142 mm diameter pressure filtration device with air pressurization and Duropore (0.45 micron) filter paper. The filter cakes are rinsed twice with THF or heptane prior to depressurizing and opening the device. After the filtrations are complete, the filter papers are dried under vacuum at 70°C, cooled to room temperature and weighed to determine the insoluble portions. The THF soluble material is quantitatively sampled for gas chromatographic (GC) determination of the reaction solvent recovery, including both phenanthrene and DHP. The THF is removed from the THF solubles by rotary evaporation prior to determining the heptane conversion.

The quantity of gases (CO, CO_2, CH_4, C_2H_4) produced in a reaction is calculated using the post-reaction vessel temperature and pressure with the ideal gas law and the mole percent in the gas sample as determined using a Carle GC and standard gas mixtures.

Factorial Experimental Design and Analysis. The factorial experimental design (Figure 1) that was chosen for this project evaluates the effects of three variables at two levels: time (20 and 60 minutes), temperature (350 and 400°C), and catalyst loading (0 and 1 wt% based on as-received coal). With this full factorial experimental design, the experimental results are evaluated for all combinations of levels of the three variables so that 2^3 evaluations are required. Additional reactions are also performed at the center point of this cubic design. An Analysis of Variance (ANOVA) is performed to estimate the effects of the experimental variables, and to statistically test their significance. Replication of the experiments is used to estimate measurement error and to reduce its effect on the estimated effects of the variables. Models are constructed using the estimates of the effects of the variables to calculate the expected experimental results for specified sets of reaction conditions[4]. The controlled factors used in the ANOVA are the measured average reaction temperature, measured reaction time, and the actual weight of catalyst used.

Standard Catalyst. Pyrite obtained from Johnson-Matthey was used as the standard catalyst for comparison with the novel catalysts. The surface area of the pyrite is 0.7m^2/g as determined using BET techniques. An x-ray diffraction pattern showed no evidence of any phases other than pyrite.

University of Pittsburgh Catalyst. This catalyst was supplied by I. Wender and V. Pradhan of the Department of Chemical and Petroleum Engineering at the University of Pittsburgh. The testing of this catalyst included a pretreatment step that was defined by the supplier and performed at Sandia just prior to testing. It involved heating the catalyst in a muffle furnace to <450°C for one hour. The catalyst was removed from the furnace and quickly transferred to the reactor to minimize exposure to air. Reactions were performed with a 2:1 sulfur to catalyst ratio on a weight basis.

Results and Discussion

The analysis of the test procedures and the factorial experimental design using pyrite as the catalyst and DHP as the reaction solvent identified temperature, time and the time-temperature interactions as the only parameters responsible for changes in conversion within the boundaries of the cube; catalytic effects were not detected[3]. There were two possible explanations for the lack of catalytic effects: either the coal or the hydrogen donor was too reactive. The pyrite was not considered to be a cause of the lack of catalytic effects because pyrite is a well-established catalyst for coal liquefaction[5], and this pyrite is very pure. Because the coal was specifically chosen for use with PETC's Fine-Particle Catalyst Development Program due to its desirable properties, it was decided to reevaluate the use of DHP as the reaction solvent. One very important function of a catalyst in coal liquefaction is to hydrogenate the reaction solvent[6] so that hydrogen is available to stabilize products of cracking reactions and thus prevent retrogressive reactions. With DHP, it was assumed that there was more than enough hydrogen available so that the catalytic effects of pyrite were not observed.

Evaluation of the Reaction Solvent. To evaluate the effect of the reaction solvent, thermal and catalytic experiments were performed at 400°C for 60 minutes with mixtures of DHP and phenanthrene. The total amount of solvent was kept constant at 3.34g to help ensure good mixing of the catalyst and coal. Results of the experiments (Figure 2) show that with a 1:1 DHP:phenanthrene ratio there is no evidence of catalytic activity. The conversions are similar to those obtained with only DHP as the solvent indicating that there is still sufficient hydrogen available. At a 1:3 ratio, a significant difference in THF conversion is observed between thermal and pyrite-catalyzed reactions. The conversions are also decreased compared to those obtained with a 1:1 ratio. This indicates that the amount of donatable hydrogen is decreasing. The maximum difference between thermal and pyrite-catalyzed reactions is observed when phenanthrene is the only reaction solvent used. In this case, pyrite catalysis causes an increase in THF conversion from about 57% to about 72%, and there may also be a small increase in heptane conversion. The conversions are significantly lower with phenanthrene as compared to those obtained when some DHP is present in the solvent. This demonstrates the importance of having a good hydrogen donor solvent in coal liquefaction. However, for purposes of comparing catalysts, it was decided that the best procedure would be the one that showed the largest catalytic effects. Therefore, the evaluation of the factorial experimental design was repeated with phenanthrene instead of DHP.

Evaluation of the Factorial Experimental Design with Phenanthrene. The evaluation of the factorial experimental design using phenanthrene as the reaction solvent was performed by a single operator. Replicates were

performed at all nine sets of reaction conditions. Due to problems with the gas analyses, only three experimental results were obtained: measured THF and heptane conversions, and the amount of DHP in the product. The measured values related to these experiments are given in Table 1. Standard deviations for reaction temperatures are routinely <1°C. Reactor heat up and quench times are about 3 minutes each. Recoveries of the reaction solvent as determined by GC analysis include quantification of both phenanthrene and DHP formed by hydrogenation of the phenanthrene. The amount of DHP in the product is monitored because it may give information on relative hydrogenation activities of catalysts. This issue will be revisited as more catalysts are evaluated.

Results of the statistical analyses of these reaction results are given in Tables 2 and 3. These tables show calculated estimates of the effects of the variables and the interactions among variables over the region bounded by the cube, calculated estimates of the mean values of the reaction results at the nine sets of reaction conditions, standard errors of the estimates, the means of the measured values in Table 1, and R^2 values for the fit of the model to the data. The constant represents the estimate of the reaction results when all variables are at their low levels: temperature=350°C, time=20 minutes, and catalyst loading=0%. The variables with statistically significant effects are listed under the constant; the larger the estimated value, the greater the effect. The estimate of experimental error, which is presented as a standard deviation, accounts for all variability in the data not accounted for by the fixed and random effects of the model. Included in this estimate are variabilities due to measurement, process and material inconsistencies and modeling inadequacies. The estimates of reaction results at the nine sets of reaction conditions are calculated from the model and can be compared to the means of the measured values. The standard errors of the estimated results at cube corners are derived from the experimental error, which pertains to a single measurement.

The R^2 values for these analyses range from 0.96 to 0.98. The calculated THF conversions range from 26.4% at 350°C for 20 minutes without catalyst to 73.4% at 400°C for 60 minutes with 1% catalyst. Contributions to the 47% difference between these two results are 24.2% for temperature, 10.1% for a catalyst-time interaction, 8.3% for catalyst, and 4.3% for time. Thus temperature has the largest effect on THF conversion. In contrast to reactions with DHP, the pyrite has a statistically significant catalytic effect. One of the contributers to the experimental error is the nonlinearity of THF conversion at the center point of the cube as observed by comparing the estimated and measured values for 375°C, 40 minutes with 0.5% catalyst. For the heptane conversions, temperature has the largest effect, and there is no significant catalytic effect. The heptane conversion is more linear near the center point than the THF conversion. The complicated model obtained for DHP in the product results from the fact that large values occur only when all three variables are at their high levels. To adequately fit this behavior, the full factorial model, including the three-way interaction term, is required. These results show that pyrite causes some hydrogenation of the phenanthrene to DHP.

Procedure for Estimating Experimental Results from the Linear Model. To use one of the linear models in Tables 2 or 3 to determine an estimate for an experimental result within the cube, first calculate proportional levels for each variable that has a significant effect. For example, to calculate THF

conversion for a reaction at 375°C for 40 minutes with 0.5% catalyst (see Table 2):

$$p_{TIME}=(40min-20min)/(60min-20min)=0.5$$
$$p_{TEMP}=(375°C-350°C)/(400°C-350°C)=0.5$$
$$p_{CAT}=(0.5wt\%-0wt\%)/(1.0wt\%-0wt\%)=0.5$$

The two calculated p's are used in the following equation:

$$K + p_{TIME}*a + p_{TEMP}*b + p_{CAT}*c + p_{CAT}*p_{TIME}*d$$

where K is the estimated constant (26.4%), a is the estimated time effect (4.3%), b is the estimated temperature effect (24.2%), c is the estimated catalytic effect (8.3%), and d is the estimated catalyst-time interaction (10.1%). The calculated THF conversion is 47.3 as shown in Table 2. For calculating a result for any point within the region bounded by the cube, the p values will range from 0 to 1. Extrapolation beyond the limits of the cube is usually not recommended.

Evaluation of the University of Pittsburgh's Sulfated Iron Oxide Catalyst. The measured experimental results obtained from testing the University of Pittsburgh's sulfated iron oxide catalyst using the factorial experimental design with phenanthrene are given in Table 4. Testing of this catalyst was performed separately by two operators one of whom had done the evaluation of pyrite. Replicates were performed at all nine sets of reaction conditions. Standard deviations for reaction temperatures are routinely <1°C; reactions with standard deviations >1.5°C were not used in the analysis and were repeated. Reactor heat up and quench times are about 3 minutes each. Recoveries of the reaction solvent as determined by GC analysis include quantification of both phenanthrene and DHP formed by hydrogenation of the phenanthrene; the recoveries are routinely greater than 90%.

Results of the statistical analyses of these reaction results are given in Tables 5 and 6. The R^2 values for these analyses range from 0.90 to 0.98. The calculated THF conversions range from 28.8% at 350°C for 20 minutes without catalyst to 82.3% at 400°C for 60 minutes with 1% catalyst. Contributions to the 53.5% difference between these two results are 24.9% for temperature, 15.1% for a catalyst, 9.4% for time, and 4.1% for the catalyst-time interaction. Temperature has the largest effect on THF conversion as was also observed with pyrite. The catalytic effect is the second largest effect and almost double the effect obtained with pyrite. One of the contributers to the experimental error is the nonlinearity of THF conversion at the center point of the cube as observed by comparing the estimated and measured values for 375°C, 40 minutes with 0.5% catalyst; this was also observed with the pyrite results. For the heptane conversions, temperature has the largest effect followed by the time-temperature interaction and the effect of time. There is no significant catalytic effect. The heptane conversion is more linear near the center point than the THF conversion. As observed with the pyrite results, the DHP analysis gave a complicated model that required all possible interactions. These results show that the catalyst-time interaction and the catalyst-temperature interaction have the largest effects on DHP concentration. The catalyst effect and temperature effect are the next largest contributors to DHP.

Statistical analysis of the gas yield shows that temperature has the largest effect followed by the time-temperature interaction and the time effect. There is no significant effect of catalyst on gas yield. The non-hydrogen, gases (excluding H_2S) detected in the reaction products were CO_2, CO, CH_4, and C_2H_6. Reactions at 350°C for 20 minutes only yield 0.14 mol% CO_2, 0.04 mol% CH_4, and 0.01 mol% CO. At 350°C for 60 minutes, CO_2 is about 0.25 mol%, CH_4 is 0.08 mol%, CH_2H_6 is 0.02 mol% and CO is 0.02 mol%. At 400°C for 20 minutes, CO_2, CH_4, CO and C_2H_6 are about 0.39, 0.27, 0.09 and 0.11 mol% respectively. At 400°C for 60 minutes, CO_2, CH_4, CO and C_2H_6 are about 0.55, 0.52, 0.11, and 0.22 mol% respectively.

In all of these analyses, the operator standard deviation is always small compared to the experimental error. These results show there is good reproducibility both between operators and by each operator and thus indicate that there are no systematic differences in the procedures used by the operators.

Comparison of the Results from Pyrite and the University of Pittsburgh's Catalyst. Comparison of the results of testing pyrite with the results of testing the University of Pittsburgh's catalyst shows some significant differences. Testing of the commercially available pyrite showed an 8.3% higher THF conversion with pyrite addition at 350°C for 20 minutes than obtained in a thermal reaction at the same conditions. Evaluation of the University of Pittsburgh's catalyst gave a 15.1% higher conversion at these same conditions. Comparison of the DHP concentrations at the end of the reactions also indicates higher activity for the University of Pittsburgh's catalyst at the lower severity conditions. At 350°C for 20 minutes pyrite addition gave a 0.1% increase in DHP, whereas the University of Pittsburgh's catalyst gave a 0.54% increase. At 400°C for 60 minutes, pyrite gave an 18.5% higher THF conversion than a thermal reaction and the University of Pittsburgh's catalyst gave a 19.3% higher conversion. At 400°C for 60 minutes, both catalysts gave similar DHP increases: 2.8% for pyrite and 2.9% for the University of Pittsburgh's catalyst. Neither of these differences are statistically significant at the 0.10 level. This indicates that the University of Pittsburgh's catalyst is more reactive at lower temperatures than pyrite. Neither catalyst had a significant effect on heptane conversion.

Conclusions

The results of this work show that use of a good hydrogen donor such as DHP can mask the effects of a catalyst, whereas the use of a non-hydrogen donor such as phenanthrene enables significant catalytic effects to be observed. The use of an experimental design gives statistical information on the effects of all variables that are evaluated as well as the interactions among the variables, thus enabling evaluation of the sensitivity of catalytic activity to time and temperature. Both pyrite and the University of Pittsburgh's sulfated iron oxide catalyst show significant catalytic effects at all conditions evaluated using the factorial experimental design. The main differences between these two catalysts are that the University of Pittsburgh's catalyst show significantly higher THF conversion and higher DHP concentrations at the lower severity operating conditions. Future work will include using the test procedure developed with phenanthrene to continue evaluating the many fine-particle size catalysts being developed in PETC's program. Additional work will evaluate methods for characterizing the heptane solubles and the THF and heptane insoluble materials and for determining

hydrogen usage in these reactions. Use of an expanded factorial experimental design to determine effects of additional variables such as hydrogen pressure will be evaluated.

Acknowledgement

This work was supported by the U.S. Department of Energy under contract DE-AC04-76DP00789. We would like to express our thanks to Richard Jensen and Jeff Kawola for performing some of the experimental work associated with this project. We would also like to thank Mike Baird and Malvina Farcasiu of PETC for the many helpful technical and programmatic discussions.

References

1. Huffman, G. P.; Ganguly, B.; Zhao, J.; Rao, K. R. P. M.; Shah, N.; Feng, Z.; Huggins, F. E.; Taghiei, M. M.; Lu, F.; Wender, I.; Pradhan, V. R.; Tierney, J. W.; Seehra, M. S.; Ibrahim, M. M.; Shabtai, J.; Eyring, E. M. Energy Fuels 1993, 7, 285-296.
2. Pradhan, V. R.; Tierney, J. W.; Wender, I. Energy Fuels 1991, 5, 497-507.
3. Stohl, F. V.; Diegert, K. V. Submitted to Energy & Fuels.
4. John, P. W. M., Statistical Design and Analyses of Experiments; MacMillan Co., 1971.
5. Stephens, H. P.; Stohl, F. V.; Padrick, T. Proc. Int'l. Conf. on Coal Sci., Dusseldorf, Germany, Sept. 7-9, 1981, pp. 368-373
6. Neavel, R. C. Fuel 1976, 55, 237-242.

Table 1. Measured experimental results with pyrite

TEMP (°C)	TIME (min)	CAT (mg)	THF CONV[a]	HEPTANE CONV[a]	DHP %[b]
350.1	21.5	0	24.3	1.5	0.40
350.3	20.0	0	29.3	1.6	0.44
351.0	20.5	0	27.6	1.7	0.27
351.2	60.0	0	31.0	6.9	0.50
350.0	60.5	0	28.9	2.4	0.54
401.0	20.0	0	48.3	17.0	0.91
401.0	20.0	0	48.9	17.6	0.83
399.3	61.0	0	53.1	21.5	1.21
400.0	60.5	0	54.9	24.0	NA[c]
374.6	39.5	8.1	52.0	13.8	0.85
375.4	40.0	8.6	53.3	13.3	1.28
374.6	40.0	9.2	52.7	13.7	0.97
374.8	43.0	8.9	49.0	10.8	1.04
350.2	20.0	16.6	32.9	2.6	0.54
350.3	20.5	17.3	33.0	2.0	0.48
349.7	60.0	17.0	48.2	7.2	1.32
350.2	60.0	16.8	47.9	5.7	1.34
399.7	20.0	17.8	60.6	17.9	1.84
399.3	20.0	16.7	59.5	16.8	1.51
399.9	20.0	16.6	57.0	16.0	1.51
399.3	60.5	17.2	74.6	29.4	4.16
399.2	61.0	17.5	73.4	27.2	4.27
399.6	60.0	16.6	72.2	27.0	3.55

a dmmf coal basis
b percent of DHP in recovered reaction solvent
c NA = not available

Table 2: Results of the statistical analyses of the measured THF and heptane conversion data from reactions performed with pyrite.

	THF Conversion			Heptane Conversion		
Parameter	Model Estimate	Measured Averages	Standard Error	Model Estimate	Measured Averages	Standard Error
Constant	26.4		1.3	1.8		0.8
Time	4.3		1.8	3.6		1.3
Temperature	24.2		1.3	15.2		1.2
Catalyst	8.3		1.7	0		
Time, Temp Inter.	0			5.3		1.7
Catalyst-time int.	10.1		2.4	0		
Experimental Error	2.7			1.9		
350, 20 min, 0%	26.4	27.1	1.3	1.8	1.6	0.8
350, 60 min, 0%	30.7	30.0	1.4	5.5	4.6	0.9
400, 20 min, 0%	50.6	48.6	1.4	17.0	17.0	0.8
400, 60 min, 0%	54.9	54.0	1.5	25.9	22.7	0.8
375, 40 min,0.5%	47.3	51.7	0.6	12.5	12.9	0.4
350, 20 min, 1%	34.7	33.0	1.4	1.8	2.3	0.8
350, 60 min, 1%	49.1	48.0	1.4	5.5	6.4	0.9
400, 20 min, 1%	58.9	59.0	1.3	17.0	16.9	0.8
400, 60 min, 1%	73.4	73.4	1.3	25.9	27.9	0.8
R^2	0.97			0.96		

Table 3: Results of the statistical analyses of DHP in the product from reactions performed with pyrite.

	DHP in Product		
Parameter	Model Estimate	Measured Averages	Standard Error
Constant	0.33		0.12
Time	0.13		0.19
Temperature	0.47		0.19
Catalyst	0.11		0.19
Time-Temp. Inter.	0.15		0.32
Time-Cat. Inter.	0.69		0.28
Temp.-Cat. Inter.	0.66		0.26
Time-Temp.-Cat. Inter.	1.33		0.41
Experimental Error	0.21		
350, 20 min, 0%	0.33	0.37	0.12
350, 60 min, 0%	0.45	0.52	0.15
400, 20 min, 0%	0.80	0.87	0.14
400, 60 min, 0%	1.08	1.21	0.20
375, 40 min,0.5%	1.23	1.04	0.05
350, 20 min, 1%	0.44	0.51	0.14
350, 60 min, 1%	1.26	1.33	0.14
400, 20 min, 1%	1.57	1.62	0.12
400, 60 min, 1%	3.88	3.99	0.12
R^2	0.98		

Table 4. Measured experimental results with the University of Pittsburgh's catalyst

OPERATOR	TEMP (°C)	TIME (min)	CAT (mg)	THF CONV[a]	HEPTANE CONV[a]	DHP %[b]	GAS (%DMMF)
1	350.5	20.5	0	32.7	10.4	0.24	0.40
2	351.4	20.0	0	26.9	2.3	0.40	0.40
2	350.7	20.0	0	27.3	1.9	0.38	0.37
2	351.2	20.0	0	29.2	2.4	0.00	0.34
1	350.6	61.0	0	35.1	4.7	0.86	0.65
1	350.7	60.0	0	36.2	4.1	0.90	0.95
2	350.4	60.0	0	43.3	10.9	0.80	0.68
2	350.4	60.0	0	38.6	8.6	0.76	0.65
2	350.9	60.0	0	39.2	8.0	1.04	0.61
1	399.9	20.0	0	50.9	18.1	1.22	1.33
1	401.1	20.5	0	50.8	17.0	1.20	1.37
2	399.4	20.0	0	52.4	19.2	1.09	1.20
2	399.6	20.0	0	51.9	16.9	1.15	1.33
1	399.7	60.0	0	59.7	24.1	2.55	NA
1	399.8	60.0	0	61.1	27.0	2.36	2.05
2	400.6	60.0	0	60.9	25.2	2.28	2.30
2	400.5	60.0	0	62.1	27.5	2.34	1.84
1	374.4	41.0	8.4	60.6	10.9	2.79	0.87
1	375.3	40.0	8.4	60.4	14.4	2.63	0.90
1	375.0	40.0	8.4	59.8	13.8	2.51	NA
1	375.9	40.0	8.1	55.2	11.1	2.36	0.95
2	375.9	40.5	8.7	62.8	17.1	2.60	0.98
2	374.8	40.0	8.6	63.4	23.3	2.13	0.68
2	375.1	40.0	8.7	58.4	16.1	2.14	0.82
1	349.3	21.0	16.7	39.9	5.2	0.97	0.36
2	351.4	20.5	17.1	41.1	2.0	0.96	0.32
2	351.4	20.0	18.1	41.8	4.7	0.94	0.29
1	349.4	60.5	16.7	55.0	4.9	2.81	0.52
1	349.7	60.0	16.6	56.7	6.5	3.17	0.76
2	350.6	60.0	17.7	59.9	11.9	2.85	0.54
2	350.1	60.5	17.2	56.3	4.8	2.93	0.59
1	400.3	20.0	16.7	67.8	19.3	3.25	1.12
1	399.5	20.5	16.7	67.0	18.1	3.15	1.18
2	400.1	20.0	16.4	74.9	19.3	3.27	1.37
2	400.3	20.0	16.5	69.6	19.5	3.21	1.41
2	400.8	20.0	16.0	69.0	18.5	3.14	1.44
2	400.5	20.0	17.9	70.2	19.1	3.29	1.39
1	400.5	60.0	17.0	81.6	31.0	5.54	1.90
2	400.5	60.5	17.2	82.8	33.8	5.50	2.02
2	400.3	60.0	17.1	80.7	30.6	5.09	1.88

a dmmf coal basis
b percent of DHP in recovered reaction solvent
c NA = not available

Table 5: Results of the statistical analyses of the measured THF and heptane conversion data from reactions performed with the University of Pittsburgh's catalyst.

	THF Conversion			Heptane Conversion		
Parameter	Model Estimate	Measured Averages	Standard Error	Model Estimate	Measured Averages	Standard Error
Constant	28.8		1.6	4.2		1.2
Time	9.4		1.9	2.9		1.5
Temperature	24.9		1.3	14.2		1.5
Catalyst	15.1		1.8	0		
Time, Temp Inter.	0			7.1		2.1
Catalyst-time int.	4.1		2.6	0		
Operator Error	0.6			0.9		
Experimental Error	3.7			2.9		
350, 20 min, 0%	28.8	29.0	1.6	4.2	4.9	1.2
350, 60 min, 0%	38.2	38.5	1.3	7.0	7.3	0.9
400, 20 min, 0%	53.6	51.5	1.5	18.4	17.8	0.9
400, 60 min, 0%	63.0	60.9	1.4	28.4	25.9	1.1
375, 40 min,0.5%	54.5	60.1	0.6	14.5	15.2	0.5
350, 20 min, 1%	43.9	40.9	1.5	4.2	4.0	1.2
350, 60 min, 1%	57.4	57.0	1.4	7.0	7.0	0.9
400, 20 min, 1%	68.7	69.8	1.3	18.4	19.0	0.9
400, 60 min, 1%	82.3	81.7	1.5	28.4	31.8	1.1
R^2	0.94			0.90		

Table 6: Results of the statistical analyses of gas yields and DHP in the product from reactions performed with the University of Pittsburgh's catalyst.

	Gas Yield			DHP in Product		
Parameter	Model Estimate	Measured Averages	Standard Error	Model Estimate	Measured Averages	Standard Error
Constant	0.29		0.06	0.42		0.11
Time	0.33		0.08	0.45		0.15
Temperature	0.99		0.08	0.79		0.15
Catalyst	0			0.55		0.16
Time, Temp Inter.	0.33		0.11	0.77		0.20
Cat, Time Inter	0			1.51		0.20
Cat, Temp Inter	0			1.50		0.20
Cat,Time,Temp Inter	0			-0.62		0.28
Operator Error	0			0.09		
Experimental Error	0.14			0.20		
350, 20 min, 0%	0.29	0.39	0.06	0.42	0.34	0.11
350, 60 min, 0%	0.62	0.71	0.05	0.87	0.83	0.09
400, 20 min, 0%	1.28	1.31	0.04	1.21	1.17	0.10
400, 60 min, 0%	1.94	2.06	0.06	2.43	2.38	0.10
375, 40 min,0.5%	1.04	0.87	0.02	2.18	2.45	0.03
350, 20 min, 1%	0.29	0.32	0.06	0.97	0.96	0.11
350, 60 min, 1%	0.62	0.60	0.05	2.92	2.94	0.09
400, 20 min, 1%	1.28	1.32	0.04	3.25	3.22	0.08
400, 60 min, 1%	1.94	1.93	0.06	5.35	5.38	0.11
R^2	0.94			0.98		

Figure 1: Factorial Experimental Design

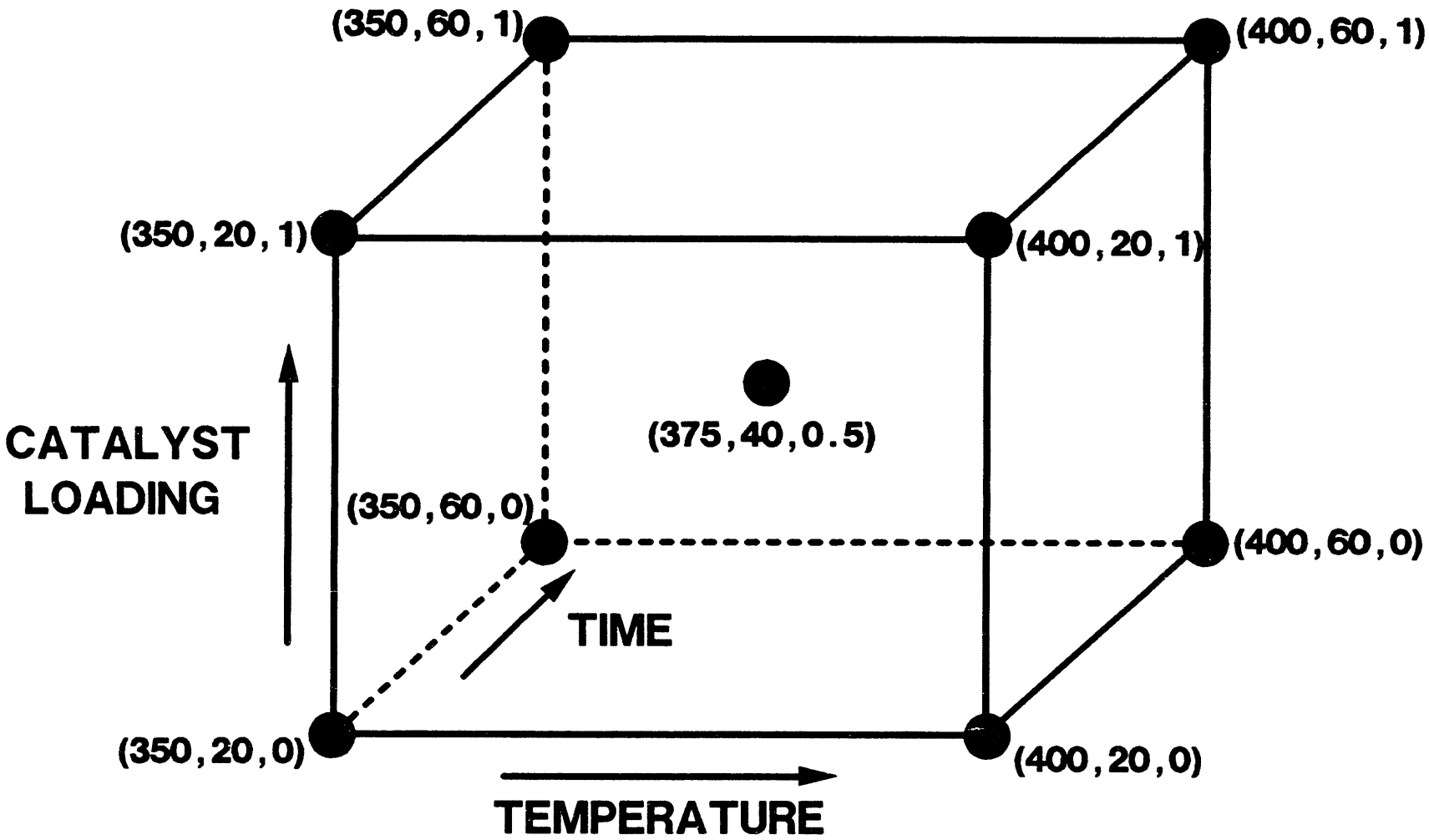

(TEMPERATURE = °C; TIME = MINUTES; CATALYST LOADING = WT % AR COAL)

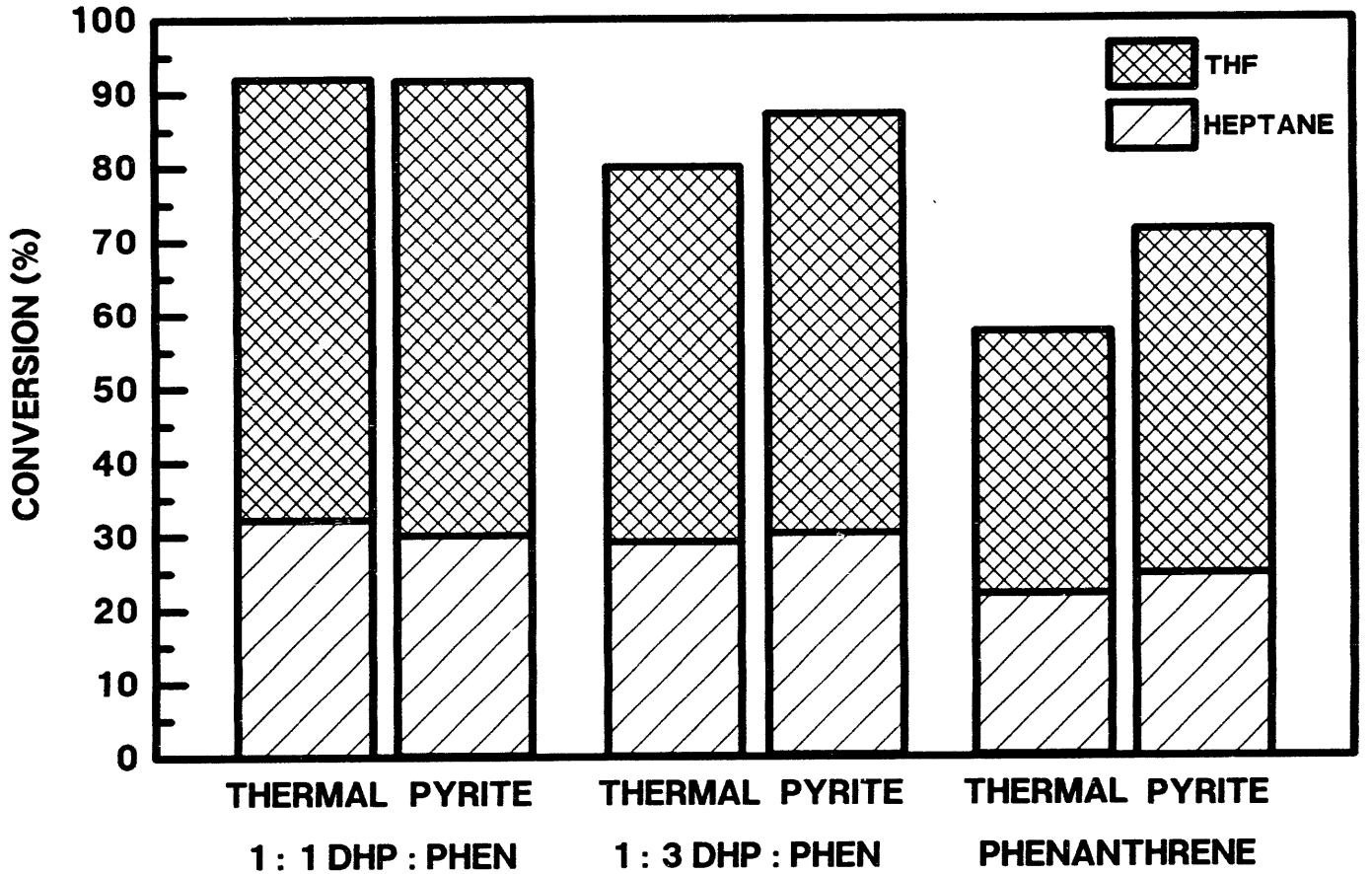

Figure 2: Effects of varying the DHP : phenanthrene ratio

GAS-TO-LIQUIDS

DEVELOPMENT OF CERAMIC MEMBRANES FOR PARTIAL OXYGENATION OF HYDROCARBON FUELS TO HIGH-VALUE-ADDED PRODUCTS*

U. Balachandran, S. L. Morissette, J. T. Dusek, R. L. Mieville, and R. B. Poeppel
Energy Technology Division
Argonne National Laboratory
Argonne, IL 60439

and

M. S. Kleefisch, S. Pei, T. P. Kobylinski, and C. A. Udovich
Amoco Research Center
Naperville, IL 60566

September 1993

Paper to be published in Proc. of Coal Liquefaction and Gas Conversion Contractors' Review Conference, Sept. 27-29, 1993, Pittsburgh, PA.

*Work at Argonne National Laboratory is supported by the U.S. Department of Energy, Pittsburgh Energy Technology Center, under Contract W-31-109-Eng-38.

DEVELOPMENT OF CERAMIC MEMBRANES FOR PARTIAL OXYGENATION OF HYDROCARBON FUELS TO HIGH-VALUE-ADDED PRODUCTS

U. Balachandran, S. L. Morissette, J. T. Dusek, R. L. Mieville, and R. B. Poeppel
Energy Technology Division
Argonne National Laboratory
Argonne, IL 60439

and

M. S. Kleefisch, S. Pei, T. P. Kobylinski, and C. A. Udovich
Amoco Research Center
Naperville, IL 60566

ABSTRACT

Several perovskite-type oxides (ABO_3) that contain transition metals on the B-site show mixed (electronic/ionic) conductivity. These mixed-conductivity oxides are promising materials for oxygen-permeating membranes that can operate without electrodes or external electrical circuitry. Oxides in the system La-Sr-Fe-Co-O permeate large amounts of oxygen. One could use this material for producing syngas ($CO + H_2$) by direct conversion of methane and other basic hydrocarbon gases, such as coal gas. Air can be used as oxidant in the conversion process. As oil companies search further into remote regions and to greater depths to maintain adequate oil supplies, they encounter ever-increasing amounts of natural gas or methane. Therefore, this direct electrochemical conversion technology based on dense ceramic membranes should be of great importance because it will upgrade these abundant basic hydrocarbons into high-value-added products.

Ceramic powders in the La-Sr-Fe-Co-O system are made by solid-state reaction of the constituent carbonates and/or nitrates. The chemical-phase behavior of the ceramic powders with varying stoichiometries is studied by high-temperature in-situ X-ray diffraction (XRD) as a function of oxygen partial pressure. Membrane tubes are fabricated from the calcined powders by a plastic extrusion technique. The extruded tubes are sintered and then characterized by scanning electron microscopy and XRD. Subsequently, they are evaluated in a reactor operated at ≈850°C for direct conversion of methane into syngas in the presence of a reforming catalyst. Methane conversion efficiencies of >99% are observed. We have operated some of the reactor tubes for up to ≈350 h. In this paper, we describe the critical steps in the processing and fabrication of membrane tubes, their characterization, and their performance in the conversion reactor.

INTRODUCTION

The upgrading of natural gas, containing mostly methane, to value-added products such as easily transportable fuels is driven by the abundance of natural gas discovered in remote areas and by the disparity in prices of petroleum liquids versus gas on a Btu-cost basis [1,2]. Over the past several years, extensive efforts have focused on both direct and indirect conversion of methane to value-added products, particularly easily transportable fuels [3,4]. The direct conversion routes involve some form of partial oxidation of methane to methanol, formaldehyde, or olefins. This is the most difficult approach because it is complicated by significant competitive side reactions that result in low selectivities to the desired products. Moreover, the reaction must be carried out at high temperatures in the gas phase. The reaction products are more reactive than the starting material, and the

competitive gas-phase reactions lead to deep oxidation [5]. Thus, any technological breakthrough in the direct conversion of methane could have a significant economic impact in the industrial sector. Indirect routes for methane conversion involve oxidation of methane to form syngas (CO + H_2) in a first stage either by steam reforming, direct partial oxidation, or a combination of both. The syngas is then converted into upgraded products such as paraffins, olefins, oxygenates, waxes, and mid-distillate fuels in a second stage by Fischer-Tropsch technology [6]. The indirect route, and in particular the syngas step, is usually very energy- and capital-intensive (steam reforming is highly endothermic), operating at high pressures and temperatures. The cost of syngas production by steam reforming can account for at least 60% of the integrated cost of the total plant.

Although direct partial oxidation of methane with air as the oxygen source is a potential alternative to today's commercial steam-reforming processes, downstream processing requirements cannot tolerate nitrogen (recycling with cryogenic separations is required) and therefore pure oxygen is required. The most significant cost associated with partial oxidation is that of the oxygen plant. Any new process that could use air as the feed oxidant and thus avoid the problems of recycling and cryogenic separation of nitrogen from the product stream will have a strong economic impact on the cost of a syngas plant, reflected in savings of capital and separation costs.

In this paper, we offer a technology based on dense ceramic membranes that use air as the oxidant for methane-conversion reactions. Dense ceramic membranes represent a class of materials that offer potential solutions to several problems in methane conversion. Certain ceramic

materials exhibit both electronic and ionic conductivities (of particular interest is oxygen-ion conductivity). These materials not only transport oxygen ions (functioning as selective oxygen separators) but also transport electrons back from the catalytic side of the reactor to the oxygen-reduction interface. As such, no external electrodes are required and if the driving potential of transport is sufficient, the partial oxidation reactions should be spontaneous. Such a system will operate without an externally applied potential. Oxygen is transported across the ceramic material in the form of oxygen anions and not oxygen molecules. The purity of the separated oxygen is determined by the selectivity of ceramic material for oxygen ions.

In principle, such materials can be shaped into a hollow-tube reactor, with air passed over the outside of the membrane and methane through the inside, as shown in Fig. 1. The membrane is permeable to oxygen at high temperatures, but not to nitrogen or any other gas. Thus, only oxygen from air can be transported through the membrane to the inside of the reactor surface, where it reacts with methane to generate partial-oxidation products. This precludes the need for an oxygen plant and allows the integration of separation and reaction into a single process. Depending upon the cocatalyst, an array of tailored products can be generated: syngas, methanol, formaldehyde, oxidative-coupled products, etc.

Other geometric forms of the reactor are possible and can provide substantially greater surface areas for reaction. Honeycomb or corrugated forms are possible [7], and such multilayer reactors will be required to achieve sufficient conversions and reaction rates for successful application to industrial processing. The kinetics of the partial oxidation processes can be easily regulated by the controlled addition of oxygen (oxygen flux) to the

reaction zone. Oxygen flux through a mixed conductor depends on the temperature, oxygen partial pressure differential between oxidation and reduction sides, membrane thickness, etc.

Recent reports in the literature suggest that ceramic membranes made of mixed conductors can successfully separate oxygen and nitrogen at flux rates that could be considered commercially feasible [8-16]. The classical material used in solid-state transport of oxygen is zirconia stabilized either by calcia or yttria. This system transports oxygen ions from the oxygen-rich side to the oxygen-deficit side, but electrodes are required to transfer the electrons to the reduction interface because stabilized zirconia is an effective electronic insulator. The nonconductivity of electrons makes zirconia unsuitable for commercial separation of oxygen because the need for electrodes with an external short circuit makes this system impractical. Incorporation of dopants such as TiO_2, Pr_2O_3, or Eu_2O_3 to induce electronic conductivity in zirconia has met with limited success in creating an electrodeless membrane material [10,14,15]. A successful approach has been to use other materials that contain both ionic and electronic conductivity; one class of such materials is perovskites of the ABO_3 type with dopants on the A and/or B sites [8,9,13-17].

Although recent reports have described various perovskite-type materials that could be used in partial-oxidation ceramic membrane reactors [12-16], little work appears to have focused on the problems associated with stability of the materials under reaction conditions and with fabrication of suitable reactors. It is therefore of critical concern to address these problems and to determine the stability of these materials under typical reaction conditions, as well as to find suitable fabrication methods for

reactors having sufficient physical and mechanical integrity to withstand the rigorous conditions associated with the partial–oxidation reactions of interest.

Perovskites in the system La-Sr-Fe-Co-O (LSFC) have been shown by Teraoka et al. [8,9] to not only exhibit both oxygen ionic and electronic conductivity but also appreciable oxygen permeabilities (≈2 orders of magnitude higher than that of stabilized zirconia) at temperatures of ≈800°C; these materials are thus natural candidates for methane conversion, where large quantities of oxygen are required. In the next section, we describe the processing and fabrication of hollow LSFC membrane tubes. The sintered membranes are characterized by scanning electron microscopy (SEM) and X-ray diffraction (XRD), and the tubes are then used in partial–oxidation studies to transport oxygen for syngas generation in conjunction with a precious–metal reforming catalyst. To decouple the effect of the catalyst on the membrane's oxygen–permeation properties, some of the tubes are used in a reactor without the reforming catalyst. We describe the critical steps in the processing and fabrication of membrane tubes, together with the characterization and performance of the tubes in the conversion reaction.

EXPERIMENTAL

Ceramic powders of LSFC with varying stoichiometry are made by solid-state reaction of the constituent carbonates and nitrates. Appropriate amounts of $La(NO_3)_3$, $SrCO_3$, $Co(NO_3)_2 \cdot 6H_2O$, and $Fe(NO_3)_3 \cdot 9H_2O$ are mixed and milled in methanol with ZrO_2 media for ≈15 h. After drying, the mixtures are calcined in air at ≈850°C for ≈16 h, with an intermittent grinding. After final calcination, the powder is ground in an agate mortar

and pestle; average particle size is ≈7 μm. The resulting powders are characterized by XRD, SEM, thermal analysis, and particle-size/distribution analysis. Morphology and particle-size distribution play a significant role during the fabrication of membrane tubes.

Before the membrane tubes are fabricated by plastic extrusion, the powder is mixed with several organic additives to provide enough plasticity for easy forming into various shapes while retaining satisfactory strength in the green state (i.e., before firing). This formulation, known as a slip, consists in general of a solvent, a dispersant, a binder, a plasticizer, and ceramic powder. The role of each additive is described in an earlier publication [12]. Ratios of the various constituents of a slip vary, depending on the forming process and such characteristics of the ceramic powder as particle size and specific surface area. After the slip is prepared, some of the solvent is allowed to evaporate; this yields a plastic mass that is forced through a die at high pressure (≈20 MPa) to produce hollow tubes. Tubes have been extruded with outside diameter ≈6.5 mm and lengths up to ≈30 cm. Wall thicknesses are 0.25-1.20 mm. In the green state, the extruded tubes exhibit great flexibility.

The green tubes are heated slowly (≈5°C/h) in the temperature range of 150-400°C to facilitate removal of gaseous species formed during decomposition of the organic additives. After the organics are thus removed, the heating rate is increased to ≈60°C/h and the tubes are sintered at ≈1200°C for 5-10 h. All heatings are in stagnant air. Figure 2 is a photograph of an extruded hollow tube. The sintered LSFC tubes are characterized by SEM and XRD and then used in our partial-oxidation studies to transport oxygen for syngas generation in conjunction with a

precious-metal reforming catalyst. Our experimental results support the oxygen-transport concept, with a significant tendency toward preferred oxidation. The performance characteristics of the membranes depend on the stoichiometry of the compound. Integrity of tubes fabricated with a certain range of stoichiometry of LSFC cations diminished rapidly on-stream, eventually leading to catastrophic failure. Detailed in-situ XRD experiments were done at high temperatures and in different atmospheres on materials with various stoichiometries to probe chemical-phase behavior. We have succeeded in fabricating a stable membrane that operated more than 350 h.

RESULTS AND DISCUSSION

Perovskites as a class are based on the structure of the mineral perovskite ($CaTiO_3$), which has a cubic lattice with one metal ion in the body center, the other metal ions at the corners, and the anions in the face centers [19]. A variety of substitutions of the A and B cations can occur. Replacing part of a divalent cation with a trivalent cation, or a pentavalent ion with a tetravalent ion (donor dopant), results in two types of charge compensation, namely, electronic and ionic, depending on the partial pressure of oxygen in equilibrium with the oxides [19,20]. The charge compensation in acceptor-doped oxides (i.e., substituting a divalent cation for a trivalent cation) is by electronic holes at high oxygen pressures but at low pressures it is by oxygen ion vacancies [14,21]. Ion vacancies are the pathway for oxide ions. Therefore, oxygen flux can be increased by increasing the amount of substitution of the lower-valence element for a higher-valence metal ion. The reported oxygen flux values [8,9,13-16] in

perovskites tend to follow the trends suggested by the charge compensation theory.

While the primary property of high oxygen flux appears to be feasible in a few combinations of dopants in ABO_3-type oxides, many other questions must be answered about the ideal material for a novel membrane reactor. For example, the mechanical properties of the chosen membrane must have the strength to maintain integrity at the conditions of reaction. It must also maintain chemical stability for long periods under reaction conditions. Oxygen flux, chemical stability, and mechanical properties depend on the stoichiometry of the ceramic membrane. We have varied the stoichiometry and prepared two membranes, identified as LSFC-1 and LSFC-2, and have studied their characteristics and performance in an actual conversion reactor. The results are described below.

The LSFC-1 tube sintered at ≈1200°C exhibited a grain size of ≈10 μm and a density of ≈5 g/cm^3. This tube broke into several pieces within a few minutes in the conversion reactor operated at ≈850°C. We carried out in-situ XRD experiments, using a Scintag PAD X vertical goniometer powder diffractometer equipped with a high-temperature furnace. XRD patterns were recorded at 850°C in Ar-O_2 gas mixtures. Phase behavior of LSFC-1 at 20% O_2 and 1% O_2 is shown in Fig. 3. The material is a cubic perovskite in an oxygen-rich (20% O_2) atmosphere. Once the oxygen partial pressure is lowered below 5%, however, the cubic phase transforms to an oxygen-vacancy-ordered phase. New peaks appear in the XRD, as seen in Fig. 3 (1% O_2). It is important to note that this material expands substantially after the phase transition; this can be seen from the change in the position of the Bragg peak near 32°. Evidently, this peak in the oxygen-vacancy-ordered

phase (in 1% O_2) is shifted to the low-angle (larger d-spacing) side of the corresponding peak in the cubic perovskite phase (in 20% O_2).

A detailed TGA analysis [22] shows that the oxygen content, x, of the sample in 1% O_2 is about 0.1 lower than that in a sample in 20% O_2. Dependence of the unit cell volume on the oxygen content of the sample has been established by comparing the lattice parameters. For example, the volume of the primitive perovskite cell, V_p, is 57.51 $Å^3$ for x = 2.67 and 59.70 $Å^3$ for x = 2.48. These results show that this material expands as oxygen is removed. Such behavior suggests that an electronic effect is predominant in influencing the specific volume; otherwise a simple size effect would cause the lattice to shrink. By linear interpolation of the above results, we predict that a decrease in x by 0.1 will result in an increase in V_p by ≈2%.

Based on the XRD results and the previous TGA data [22], we can obtain a clear picture about the state of the LSFC-1 membrane tube under reaction conditions. We will first discuss the operation of the membrane tube solely as an oxygen separator. In this case, high oxygen pressure is maintained outside the tube and low oxygen pressure is maintained inside the tube. Before the tube is brought up to high temperature, it has an uniform distribution of oxygen. Upon heating, the tube begins to lose oxygen that was incorporated previously in the fabrication process. Moreover, the material on the inner wall will lose more oxygen than that on the outer wall. As a result, a stable oxygen gradient is generated between the outer and inner walls. It follows that the material, depending on its location in the tube, may have different phase constituents. The likely phase representation of the tube at 850°C is shown in Fig. 4. The material is single phase in

the outer and inner zones but multiphase in the middle zone. In principle, the efficiency of oxygen permeation differs from zone to zone, and the oxygen flux passing through the membrane tube is controlled by the least-permeable zone. We believe that the inner zone is less oxygen-permeable (due to the more ordered nature of oxygen vacancies) than the outer zone. By contrast, we know little about how phase separation in the middle zone would affect the rate of oxygen permeation in this material.

The most remarkable factor, which can cause tube fracture, appears to be the lattice mismatch between the materials on the inner and outer walls of the tube. As mentioned earlier, the oxygen content of the sample in 1% O_2 atmosphere is ≈0.1 lower than the oxygen content of the sample in equilibrium with 20% O_2. Therefore, the material volume on the low-oxygen-pressure side will expand an additional 2% over that on the other wall. Such compositional expansion is equivalent to a thermal expansion of 333°C (assuming that the volumetric thermal expansion coefficient is ≈6 x 10^{-5}/°C). Considering the brittleness of oxides in this family of materials, there is no doubt that this tube will break under reactor conditions.

In comparison, sample LSFC-2 exhibits a remarkable structural stability at high temperature, as shown in Fig. 5. We found no phase transitions in this material as oxygen partial pressure was changed. Furthermore, the Bragg peaks stay at the same positions regardless of the oxygen partial pressure of the atmosphere. As a result, no appreciable strain should build up across the reactor tube. Tubes made of this material, unlike those of LSFC-1, should not fracture under reactor conditions.

Figure 6 shows the conversion data obtained with a membrane tube made of LSFC-2 and operated at 850°C for ≈70 h. A reforming catalyst was used inside the tube. The feed gas contains 80% methane and 20% argon. Argon was used as an internal calibration standard for gas analysis. Both the feed gas and the effluents were analyzed with a gas chromatograph. Air is the source of oxygen. As seen from Fig. 6, methane conversion efficiency is >98%, and CO selectivity is 90%. As expected, measured H_2 selectivity is about twice that of CO (chemical mass-balance shows that for each mole of CO, there should be two moles of H_2).

Observations by Liu et al. [23] indicate that not only the conductivity of the membrane material but also the catalytic activity of the surface or interfaces has a significant effect on the rate of oxygen permeation. The conductivity (ionic and electronic) determines the mass and charge transport rate through the membrane, while the catalytic activity controls the rate of the interfacial electrochemical reactions. To decouple the role of the catalyst in the transport of oxygen across the membrane, the LSFC-2 tube was tested without the reforming catalyst. The results from a run of ≈350 h are shown in Fig. 7. The feed gases are the same as before. In the absence of the catalyst, the oxygen transported through the membrane reacts with methane and forms CO_2 and H_2O. As seen in Fig. 7, ≈35% methane conversion efficiency was obtained and CO_2 selectivity was ≈90%. Under our operating conditions, the measured oxygen flux is ≈0.3 $scc/cm^2/min$. As mentioned earlier, oxygen flux depends on temperature, oxygen potential difference between the two sides, thickness of the membrane, etc.

Due to the reaction between methane and the oxygen permeating through the membrane, H_2 and CO are generated (in the presence of a reforming catalyst). Direct contact between the tube and the H_2 gas (CO may have the same effect) may cause the perovskite phase to lose its lattice oxygen. When a portion of the oxygen is lost, the perovskite lattice would collapse and the material would decompose and break apart. To use the LSFC membrane tube in converting methane to syngas, it appears critical to reduce the wall thickness of the tube. Once the wall of the tube is thinner, the oxygen lost from the perovskite phase to the reaction stream can be refilled by the oxygen permeating from the high-pressure side. As a result, the material in contact with the reaction stream will not be deeply reduced and hence chemical decomposition would not occur. Meanwhile, the difference in oxygen content between the two walls becomes smaller and consequently, fracturing of the tube is less likely. Thus, a thin-wall membrane tube appears to be more promising for the application of methane conversion in the future. A thin-wall membrane will also maximize the surface-area-to-volume ratio and thereby reduce the reactor size. Several suggestions have been made for manifolded monolithic systems of the type reported by Hazbun [10]. In the area of solid-oxide fuel cells, several monolithic designs have been suggested and demonstrated [24-27]; these could be adapted for the use in a monolithic reactor.

CONCLUSIONS

Long lengths of La-Sr-Fe-Co-O (LSFC) membrane tubes have been fabricated by plastic extrusion. Thermodynamic stability of the tubes is studied by high-temperature XRD measurements as a function of oxygen partial pressure. Performance of the membrane strongly depends on the

stoichiometry of the material. Fracture of certain LSFC tubes is the consequence of an oxygen gradient that introduces a volumetric lattice difference between the inner and outer walls. However, tubes made with a particular stoichiometry (LSFC-2) provide methane–conversion efficiencies of >99% in a reactor. Some of these reactor tubes have operated for up to ≈350 h. This thin-wall membrane ceramic material could prevent both fracture and chemical decomposition of the tube.

ACKNOWLEDGMENTS

Work at Argonne National Laboratory is supported by the U.S. Department of Energy, Pittsburgh Energy Technology Center, under Contract W-31-109-Eng-38.

REFERENCES

1. G. E. Keller and M. M. Bhasin, J. Catal. **73**, 9 (1982).
2. G. J. Hutchings et al., Chem. Soc. Rev. **18**, 251 (1989).
3. N. D. Spenser and C. J. Pereiva, J. Catal. **116**, 399 (1989).
4. H. D. Gesser et al., Chem. Rev. **85**, 235 (1985).
5. Y. Amenomiga et al., Catal. Rev.-Sci. Eng., **32**, 163 (1990).
6. G. Henrici-Olive and S. Olive, Angew. Chem. Int. Ed. Engl., **15**, 136 (1976).
7. U. Balachandran et al., Proc. 24th Intersociety Energy Conversion Engineering Conf., Washington, DC, **3**, 1541 (1989).
8. Y. Teraoka et al., Chem. Lett., **19**, 1743 (1985).
9. Y. Teraoka, T. Nobunaga, and N. Yamazoe, Chem. Lett., 503 (1988).
10. E. A. Hazbun, U.S. Patent 4,791,079, Dec. 13, (1988).

11. K. Omata et al., Appl. Catal., **52**, L1 (1989).

12. U. Balachandran et al., Proc. Intl. Gas Research Conf., Orlando, FL (ed. by H. A. Thompson, Government Institutes, Inc., Rockville, MD), pp. 565-573 (1992).

13. T. J. Mazanec, T. L. Cable, and J. G. Frye, Jr., Solid State Ionics, **53-56**, 111 (1992).

14. T. M. Gur, A. Belzner, and R. A. Huggins, J. Membrane Sci., **75**, 151 (1992).

15. T. L. Cable, European Patent EP 0 399 833 A1, Nov. 28, 1990.

16. T. L. Cable, European Patent EP 0438 902 A2, July 31, 1991.

17. J. B. Wiley and K. R. Poeppelmeier, J. Solid State Chem., **88**, 250 (1990).

18. R. D. Evans, "An Introduction to Crystal Chemistry," Cambridge University Press, Cambridge, England (1964).

19. N. G. Eror and U. Balachandran, J. Solid State Chem. **40**, 85 (1981).

20. U. Balachandran and N. G. Eror, J. Phys. Chem. Solids, **44**, 231 (1983).

21. N. G. Eror and U. Balachandran, J. Amer. Ceram. Soc., **65**, 426 (1982).

22. S. Pei et al., submitted to J. Amer. Ceram. Soc., 1993.

23. M. Liu et al., Proc. Intl. Gas Research Conf., Orlando, FL (ed. by H. A. Thompson, Government Institutes, Inc., Rockville, MD), pp. 183-192 (1992).

24. J. P. Ackerman and J. E. Young, U.S. Patent 4,476,198, Oct. 9, 1984.

25. T. D. Claar, D. E. Busch, and J. J. Picciolo, U.S. Patent 4,883,497, Nov. 28, 1989.

26. R. B. Poeppel and J. T. Dusek, U.S. Patent 4,476,196, Oct. 9, 1984.

27. D. C. Fee et al., U.S. Patent 4,877,506, Oct. 31, 1989.

FIGURE CAPTIONS:

Figure 1: Schematic diagram of membrane reactor for methane conversion.

Figure 2: Picture of extruded hollow LSFC tube.

Figure 3: XRD of LSFC-1 at 850°C in 1% O_2 and 20% O_2.

Figure 4: Schematic diagram of likely phase presentation of LSFC-1 tube operating between ambient-pressure O_2 and low-pressure O_2.

Figure 5: XRD of LSFC-2 at 850°C in 1% O_2 and 20% O_2.

Figure 6: Methane conversion and selectivities of CO and H_2 in LSFC-2 membrane reactor with reforming catalyst.

Figure 7: Methane conversion, CO_2 selectivity, and oxygen permeability in LSFC-2 membrane reactor without reforming catalyst.

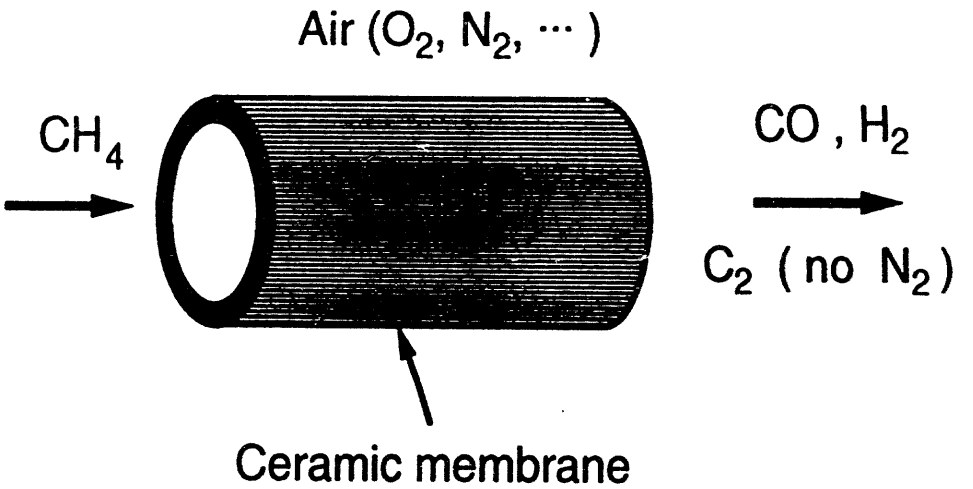
Air (O_2, N_2, ···)
CH_4
CO , H_2
C_2 (no N_2)
Ceramic membrane

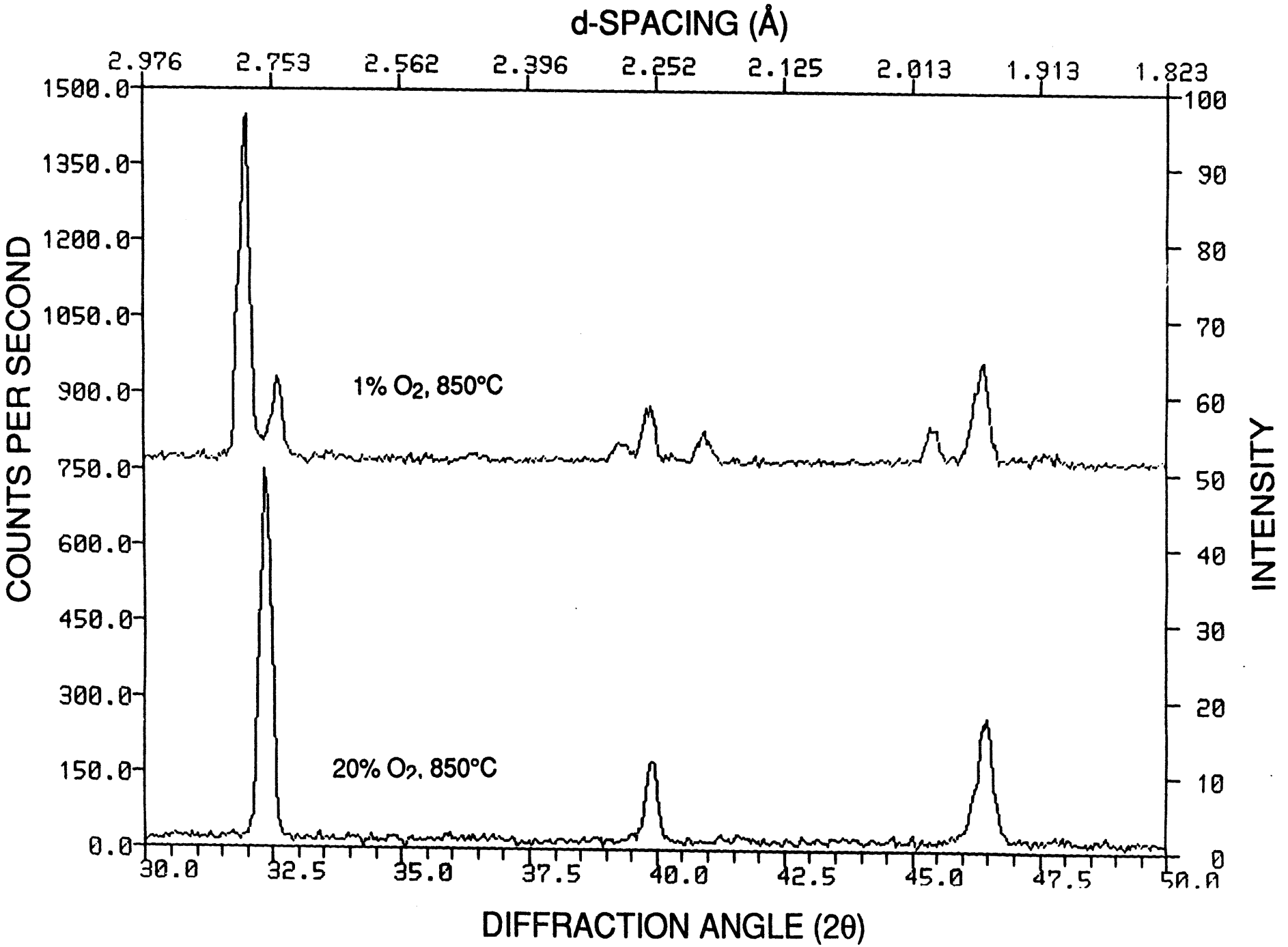
d-SPACING (Å)
2.976
2.753
2.562
2.396
2.252
2.125
2.013
1.913
1.823
COUNTS PER SECOND
1500.0
1350.0
1200.0
1050.0
900.0
750.0
600.0
450.0
300.0
150.0
0.0
INTENSITY
100
90
80
70
60
50
40
30
20
10
0
1% O2, 850°C
20% O2, 850°C
30.0
32.5
35.0
37.5
40.0
42.5
45.0
47.5
50.0
DIFFRACTION ANGLE (2θ)

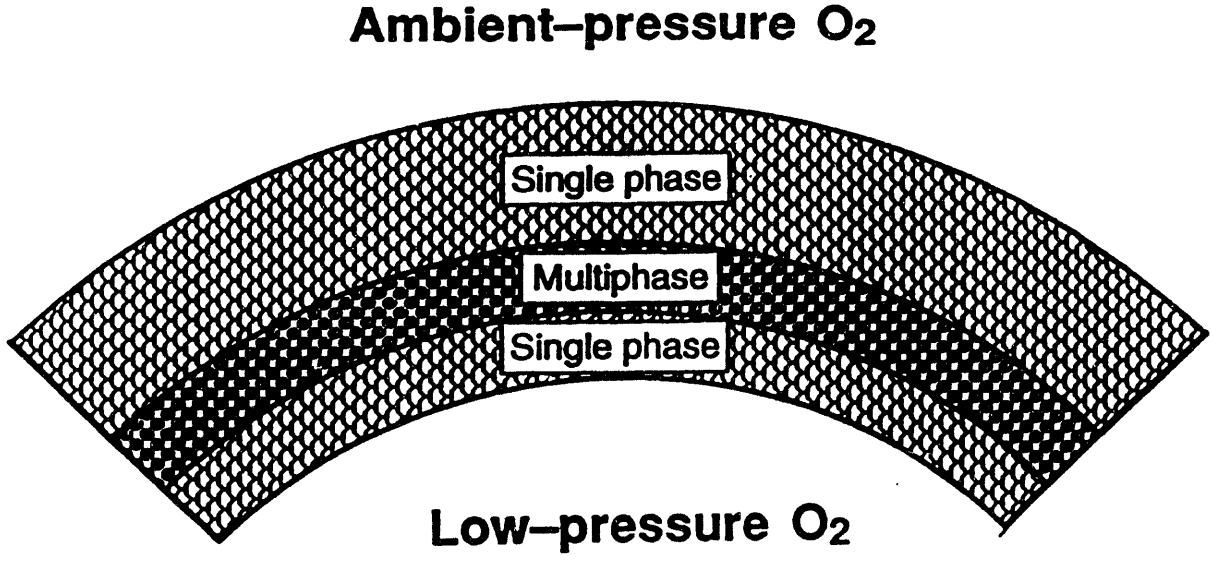
Ambient–pressure O_2
Single phase
Multiphase
Single phase
Low–pressure O_2

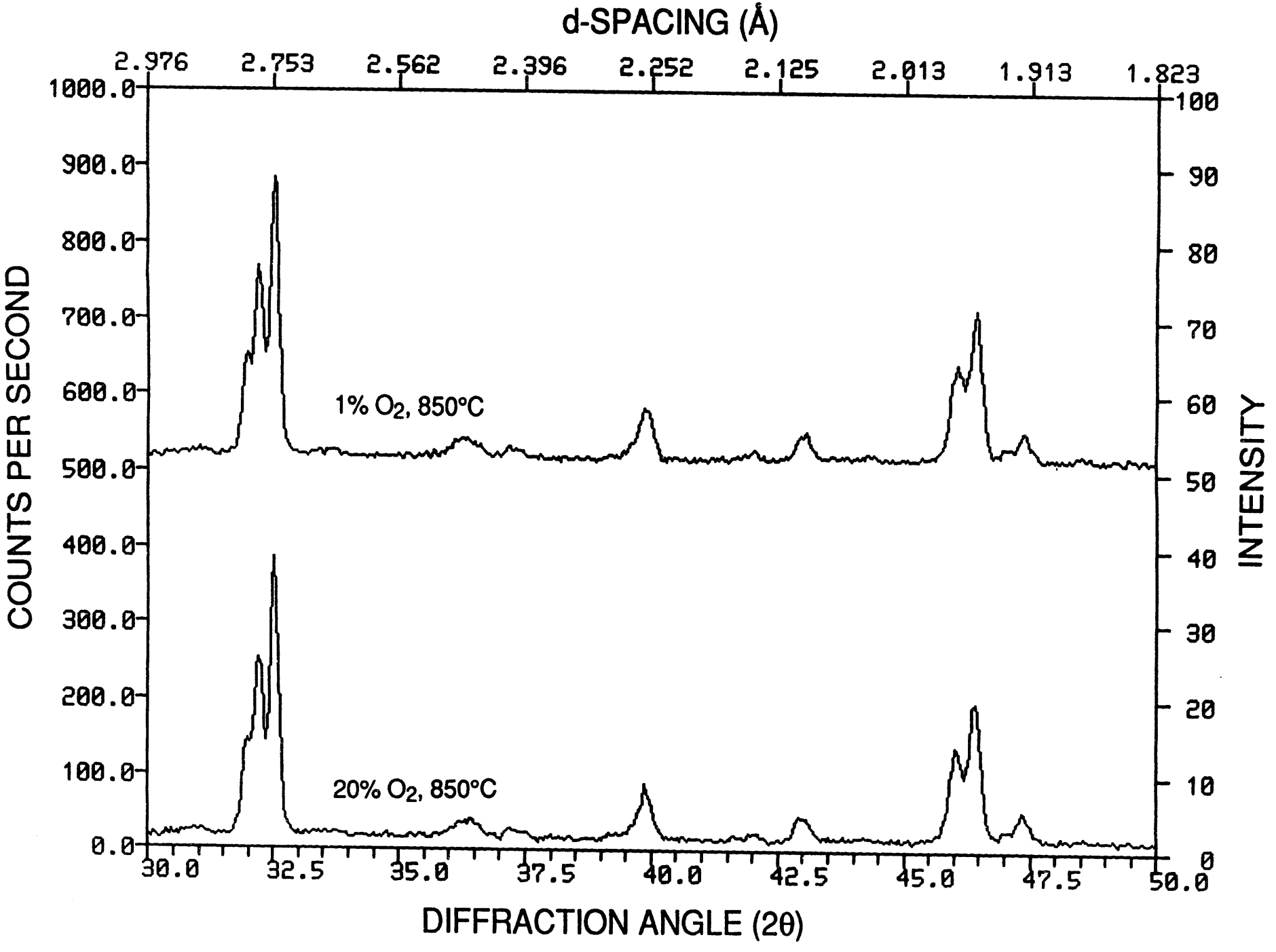
d-SPACING (Å)
2.976
2.753
2.562
2.396
2.252
2.125
2.013
1.913
1.823
1000.0
900.0
800.0
700.0
600.0
500.0
400.0
300.0
200.0
100.0
0.0
COUNTS PER SECOND
100
90
80
70
60
50
40
30
20
10
0
INTENSITY
1% O2, 850°C
20% O2, 850°C
30.0
32.5
35.0
37.5
40.0
42.5
45.0
47.5
50.0
DIFFRACTION ANGLE (2θ)

CH4/CO mole %
100
95
90
85
80
0
10
20
30
40
50
60
70
Time (h)
CH4 conversion
CO selectivity
H2 selectivity
200
195
190
185
180
175
170
165
160
Hydrogen mole %

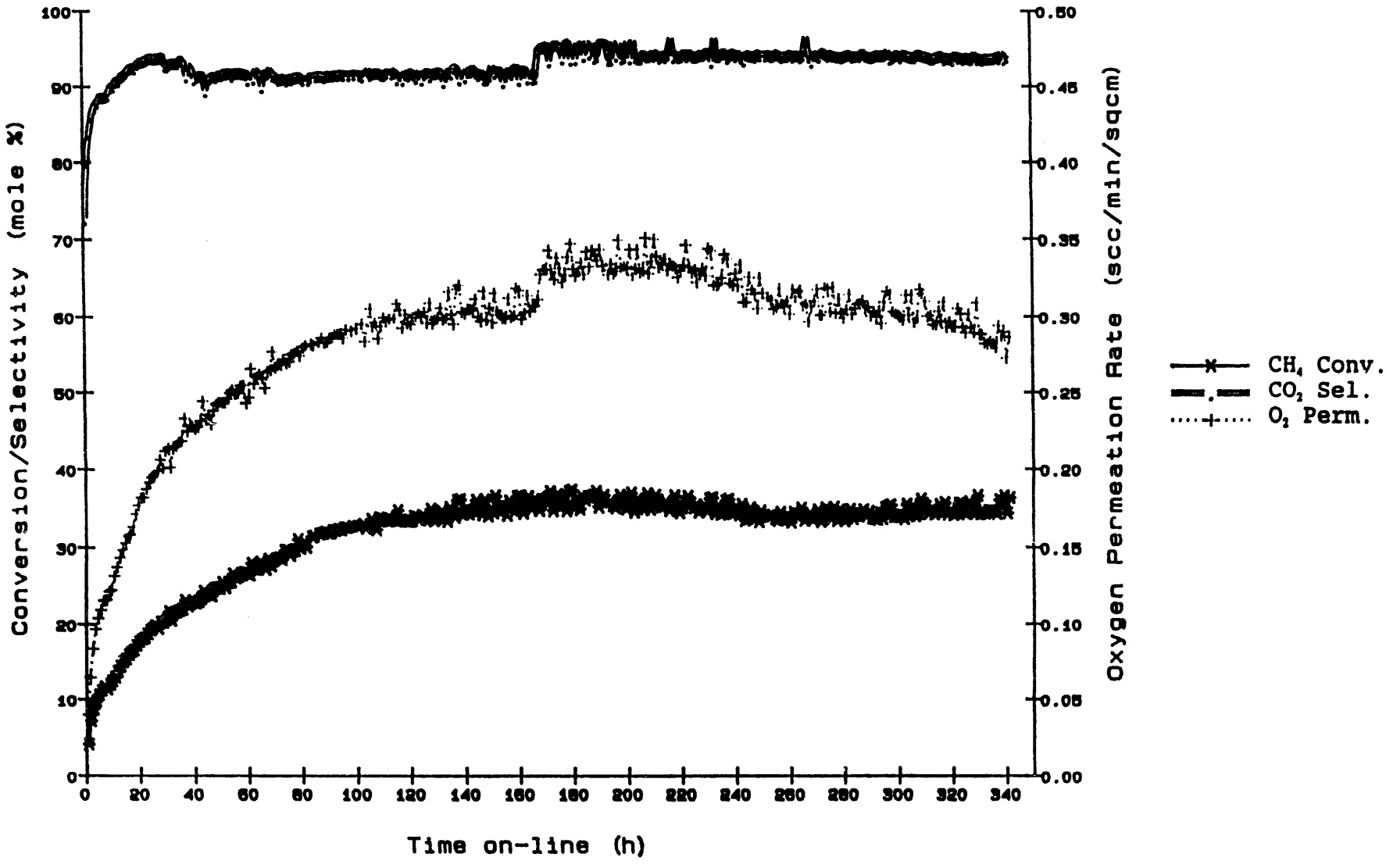
Conversion/Selectivity (mole %)
Oxygen Permeation Rate (scc/min/sqcm)
Time on-line (h)
CH4 Conv.
CO2 Sel.
O2 Perm.
0
10
20
30
40
50
60
70
80
90
100
0.00
0.05
0.10
0.15
0.20
0.25
0.30
0.35
0.40
0.45
0.50
0
20
40
60
80
100
120
140
160
180
200
220
240
260
280
300
320
340

COAL LIQUEFACTION AND GAS CONVERSION CONTRACTOR'S REVIEW CONFERENCE

CONTRACT TITLE : **Oxidative Coupling of Methane Using Inorganic Membrane Reactor**

CONTRACT NUMBER : **DE-AC22-92 PC92113**

Principal Investigators : Y.H. Ma
W.R. Moser
A.G. Dixon

Research Associates : A.M. Ramachandra
A. Boyé

Graduate Student : Y. Lu

OBJECTIVE

The overall goal of this research is to study the oxidative coupling of methane in an inorganic catalytic membrane reactor. A specific target is to achieve conversion of methane to C_2 hydrocarbons at very high selectivity and relatively higher yields than in fixed bed reactors by controlling oxygen supply through the membrane. A membrane reactor has the advantage of precisely controlling the rate of delivery of oxygen to the catalyst. This facility permits balancing the rate of oxidation and reduction of the catalyst. In addition, membrane reactors minimize the concentration of gas phase oxygen thus reducing non selective gas phase reactions, which are believed to be a main route for formation of CO_x products. Such gas phase reactions are a cause of decreased selectivity in oxidative coupling of methane in conventional flow reactors. Membrane reactors can also produce higher product yields by providing better contacting of the reactant gases and the catalyst due to the porous structure than conventional flow reactors.

Approach

In order to achieve the objective of obtaining higher conversions and higher C_2 yields, the approach followed in this work is to use various configurations of membrane reactors to control the supply of oxygen to the methane coupling reaction. Three reactor configurations are proposed to be studied. The first is a packed bed reactor where the tube containing the catalyst bed is a porous membrane. The main function of the membrane here is to allow metering of the supply of oxygen, however some loss of methane can occur. The second kind of membrane reactor will have the catalyst doped inside the membrane. Thus the actual methane coupling reaction would occur inside the membrane. Oxygen flowing in the shell side will permeate the membrane and meet methane diffusing into the membrane from the opposite side (tube side). The third type of reactor would be a dense membrane reactor. The dense membrane would be made of a material that is impervious to gases other than oxygen and thus would allow only oxygen to permeate from the shell side to the tube side. The conversion and selectivity of the coupling reaction can therefore be regulated by controlling the rate of oxygen transfer to the tube side. To complement the experimental studies and to guide the experimental work, mathematical modeling of the different reactor configurations, incorporating the kinetics of oxidative coupling of methane, will be carried out.

MEMBRANE PREPARATION AND CHARACTERIZATION

To modify commercially available porous membranes to decrease their permeance, perovskite type oxides have been used because of their electrical conductivity and oxygen permeation property. After densification of the membrane by closing the pores of the membrane completely, the dense membrane should be preferentially permeable to oxygen transfer. For the dense membrane to operate without any external electrical circuit and aid in oxygen (anion) transfer, the densification material should also be electrically conducting. Perovskite-type oxides are therefore good candidate materials for densification of porous membranes.

The oxygen semi-permeability in perovskite type oxides ($La_{1-x}A_xMO_{3-\delta}$) is correlated with the mixed conductivity of the perovskites. This mixed conductivity arises from the following : (1) the mixed valence state of the 3d transition metals, M, which results in high electron conductivity; (2) the large oxygen non-stoichiometry, which is related to the high diffusivity of the oxide ions; (3) the composition of the complex oxide. Teraoka *et al.*[1], showed the effect of the cation substitution as an increase of the rate of oxygen permeation through $La_{0.6}A_{0.4}Co_{0.8}B_{0.2}O_3$ at fixed temperature as the 'A' cation is replaced successively by Na < Sr < Ca < Ba, and the 'B' cation by Mn < Cr < Fe < Co < Ni < Cu; and finally, (4) the stoichiometry and the crystallographic structure, which, along with the composition, surface structure and morphology of the final product, are determined by the preparation procedure.

Two main synthesis routes were followed for preparing these perovskite-type oxides. The first is a mixed solid oxide process, which consists of the decomposition of precursor compounds containing the desired metal ion in air or oxygen. The second route is a solution process in which evaporation and decomposition allow intimate mixing of the metal ions in the precursors and synthesis at low temperature results in high surface areas. In preparing the perovskite for depositing in the porous membranes, we have used the following kinds of solution methods :

- the coprecipitation method : A precipitating agent is added to a solution containing the precursor compounds. The homogeneity and the degree of atomic mixing of the metal ions in the precipitates depend on the solubility products of the compounds involved.

- the sol-gel method : An amorphous gel is synthesized in ethylene glycol. The deposited gel is then dried and calcined to the oxide form.

The perovskite-type ferrites $La_{(1-x)}Sr_xFeO_{3-\delta}$ have been extensively studied. The choice of the degree of Sr substitution is based on the consideration of a good compromise between the electronic and ionic conductivities. Kim *et al.* [2] have studied the influence of Sr composition on the electrical conductivity, oxygen self-diffusion coefficient D, and oxygen vacancy concentration. Their study concluded that both electric conductivity and oxygen self-diffusion are maximized in perovskite-type oxide $La_{0.4}Sr_{0.6}FeO_{3-\delta}$ as seen in Figure 1. (i.e. $x=0.6$ in the above formula). We have synthesized the series of these Sr-substituted perovskite-type ferrites, and the XRD spectra of these compounds are presented in Figure 2. It can be seen that the perovskite structure ($x=0$) is retained fairly well until the Sr concentration reaches 0.6 ($x=0.6$). Based on these results the objective of the membrane modification is to observe the effect of different membrane modification factors on the transport mechanisms, by studying the permeation properties.

Experimental Procedure :

Membrane-supports:

The untreated ceramic membrane-supports used in our study were made of either alumina or zirconia, and were essentially meso-porous and tubular. Two types of alumina membranes were used as supports : an α-alumina membrane consisting of three layers with mean pore diameters of 2000, 8000, and 125000 Angstroms, and a gamma alumina membrane which additionally contains a thin, 50 Angstrom pore diameter, γ-alumina layer on top of the smallest pore size α-alumina membrane (see table 1 below). The zirconia membranes that were used were available with three pore sizes in the top thin layer : 200, 500, 1000 Angstroms.

Table 1. Structure of alumina membranes

LAYER	THICK (μm)	MATERIAL	PORE SIZE (Å)	POROSITY (%)
1	3-5	γ-ALUMINA	50	50
2	30	α-ALUMINA	2000	35
3	50	α-ALUMINA	8000	40
4	1,500-2,000	α-ALUMINA	125,000	40-45

Metal nitrates solution:

After trying different methods of preparation, we chose the ethylene glycol technique which allowed the synthesis of pure perovskite at low temperatures. The precursor solution of $La_{0.4}Sr_{0.6}FeO_{3-\delta}$ was prepared by dissolving the corresponding metal nitrates in ethylene glycol. In order to obtain the variations in Sr content in the perovskite-type oxides, the Sr concentrations in the solutions were varied relative to the formula equivalent, $La_{0.4}Sr_{0.6}FeO_{3-\delta}$ (0.1, 0.4, 0.6, 0.8 mol/l, see Table 2 below). X-Ray Diffraction spectra in Figure 2 show the crystallographic structure of $La_xSr_{(1-x)}FeO_3$, verifying that perovskite structure was obtained.

Table 2. Starting compositions of precursors used for preparing Sr substituted perovskite-type oxides

Formula	Amount of Precursor (gms [no. of moles])			Sample ID
$La_xSr_{(1-x)}FeO_3$	Lanthanum nitrate $La(NO_3)_3.6H_2O$ M.W. = 433.02	Strontium nitrate $Sr(NO_3)_2$ M.W. = 211.63	Iron nitrate $Fe(NO_3)_3.9H_2O$ M.W. = 404.02	After calcination
LaFeO3	4.3302[0.01]	-	4.0402[0.01]	AB102a
$LaFeO_3$	3.4642[0.008]	0.4233[0.002]	4.0402[0.01]	AB102c
$La_{0.2}Sr_{0.8}FeO_3$	2.5981[0.006]	1.2698[0.004]	4.0402[0.01]	AB102d
$La_{0.4}Sr_{0.6}FeO_3$	1.7321[0.004]	1.2698[0.006]	4.0402[0.01]	AB102b
$La_{0.2}Sr_{0.8}FeO_3$	0.8661[0.002]	1.6931[0.008]	4.0402[0.01]	AB111d
$SrFeO_3$	-	2.1163[0.01]	4.0402[0.01]	AB111b

Impregnation method :

The incipient wetness method was used for the perovskite-type oxide impregnation. This technique allows the use of either an aqueous or a non-aqueous solvent. This simple technique consists of pouring the metal precursors solution into the tube where the solute deposits directly on to the support. The main parameters are the temperature, pressure, solution concentration, configuration of the apparatus and the contact time. Unless otherwise mentioned, the impregnation is made at room temperature and atmospheric pressure. The membrane-support tube was positioned vertically and in order to minimize the effect of gravity, the tube was flipped over (turned upside down) after one half of the contact time. The contact time was kept constant at ten minutes for most of the prepared membranes. The excess liquid was then

decanted, and the tube was placed in an electrical oven in order to evaporate the solvent to obtain an amorphous gel, and then to calcine the gel to get the oxide. Based on the results obtained from the synthesis of oxide powder, a similar treatment was employed for the preparation of membranes; first, the gelation at 150°C, then drying by evaporation of the free solvent at 200°C and finally calcination at 600°C for 20 hours. The temperature is raised stepwise, maintained for two hours for every 100°C rise, between 200°C and 600°C, in order to avoid a temperature extreme change which can damage the membrane. Cooldown is at the same rate, allowing a stress-relaxation step at 100°C overnight to release the stresses created during the calcination.

Permeance measurements:

The permeation setup is of shell-and-tube configuration as shown schematically in Figure 3. Graphite string was used to seal the ceramic membrane tube to the main metallic frame of the shell. This setup can withstand temperatures up to 600°C. A pressure transducer gauge is attached to the tube side and another one is welded to the shell side in order to avoid any pressure drop created by tube fittings. The tube side exit, as well as the shell side inlet are blocked. High purity gases fed into the tube side, permeate through the membrane and flow out of the shell and the flow rate can be measured by a flow meter. This flow meter is at the atmospheric pressure; a bubble flow meter was chosen for small flows (smaller than 1 liter/min), and a wet test meter for flows between 1 and 13 liter/min. The gas permeance was measured at room temperature.

The permeances of pure gases nitrogen, helium, oxygen, and methane were measured at room temperature on both the original (unmodified) membranes and the metal oxide modified membranes. In choosing a membrane for impregnation of oxides, several options have been investigated. The commonly used ceramic membranes are alpha alumina membranes, gamma alumina membranes, zirconia membranes and porous VYCOR membranes. The choice of the membrane for impregnation will be limited essentially by the stability of its oxide phase. For example, zirconia will be limited by its tetragonal-monoclinic phase transformation, and gamma-alumina, by its allotropic transformation to obtain alpha-alumina membrane as final product. Another important factor to consider is the activity of zirconia as catalyst for the methane coupling reaction. As is well known in the literature, the zirconia membranes are not very active as catalyst, but they are useful to study the influence of support pore size, as these are available commercially with a wide range of pore size between 200 and 1000 Angstroms. The following describes our experiments with these different membranes for achieving pore closure and developing a dense membrane reactor for oxidative coupling of methane.

Alpha alumina membranes :

Alpha alumina membranes have very good high temperature stability up to 1000°C, but these α-alumina membranes are not available commercially in pore sizes less than 2000 Angstroms. Systematic studies on variation of permeance across alpha alumina membranes with different perovskite loadings have been performed. The permeance of various gases has been investigated, as well as the change in these permeance values with increasing number of perovskite depositions and the effect of using different perovskite solution concentrations. Figure 4 shows the change in permeance of nitrogen gas through a 2000 Angstrom alpha alumina membrane with increasing number of perovskite depositions. The first four consecutive depositions cause a decrease in nitrogen permeance as shown in the first figure (A). Figure (B) shows the permeance change for nitrogen gas after the 4th, 5th, 6th, 7th and 8th deposition with perovskite solution concentrations of 0.4M and 0.6M. In this and other experiments with different gases, a leveling off of permeance value was observed after about 7 depositions (saturated permeance value ≅ 3 X 10^{-6} mol/sec.m^2.Pa. in this case). Further depositions did not cause any more lowering of the permeance. Based on the premise that the higher concentrations of perovskite solutions might be too viscous to penetrate and fill the constricted pores, a set of experiments was devised where a few cycles of depositions are made at successively lower solution concentrations. Figure 5 shows the results obtained on a 2000 Angstrom pore size alpha alumina membrane where the concentrations of the perovskite solution were dropped from 0.8 M to 0.1 M and a total of 12 depositions were made. The permeance of nitrogen gas seems to have saturated at 2.5X10^{-6} mol/sec.m^2.Pa. at the end of this experiment and this is about the lowest value of permeance obtainable so far in our experiments with alpha alumina membranes. Similar results were seen with helium gas where the permeance leveled off at ≅ 6X10^{-6} mol/sec.m^2.Pa. as seen in Figure 6. In fact, the lowering of concentrations of the depositing solutions seems to be counterproductive after a few stages, since an increase in permeance is observed. The previously deposited perovskite was probably being washed away by the dilute perovskite solution. It is also possible that repeated calcination at high temperatures may change the membrane, developing cracks and thereby increasing the permeation rate.

A thermal treatment study has been carried out to observe the effect of high temperature calcinations between successive depositions. Table 3 below reports the loading (weight of perovskite deposited) after each deposition on alpha-alumina supports. The two membranes A6 and A7 are treated differently, A6 is calcined at 600°C after each deposition, while A7 is only subjected to a final calcination after the third deposition.

Table 3. Comparison of thermal treatments (successive vs. final) on perovskite loading of alumina membranes.

	MEMBRANE A6		MEMBRANE A7	
Deposition Number	Loading Material weight (g)	Thermal treatment	Loading Material weight (g)	Thermal treatment
0	0	200°C then 600°C	0	200°C
1	0.1490	"	0.2490	200°C
2	0.3213	"	0.4860	200°C
3	0.4333	"	0.6597 0.4338	200°C 600°C

From this study, we observe that the same loading weight for the oxide is obtained after three depositions and the 600°C calcination for both membranes, i.e. 0.433 gms. Furthermore, a comparable permeance is observed : about 5.2 10^{-5} mol/s.m^2.Pa for nitrogen gas after the 600°C calcination. The permeance measurements carried out on the alpha-alumina membrane A7 prior to the final calcination step demonstrated lower values. Figure 7 shows the result for the A7 alumina membrane. The permeance to nitrogen which was $\cong 1.5X10^{-5}$ mol/sec.m^2.Pa. after the third deposition jumped back to $\cong 5X10^{-5}$ mol/sec.m^2.Pa. after a thermal treatment at 600°C.

Permeances of different gases through alumina membranes have also been measured in the course of this work. Four different gases were investigated for their permeance through the membranes: Nitrogen, Oxygen, Helium and Methane. Figure 8 shows the permeance values of different gases passed through an alpha alumina membrane that has undergone four depositions of a perovskite solution (solution concentration =0.6 M).

Gamma Alumina Membranes :

Gamma alumina membranes are commercially available with a pore size of about 50 Angstroms and thickness of approximately 5 μ. Room temperature permeance of helium gas through these γ-alumina membranes was measured to be about 3.5 $X10^{-5}$ mol/sec.m^2.Pa. while

the permeance for nitrogen gas was found to be about 2.0 $X10^{-5}$ mol/sec.m^2.Pa. Permeance to various gases was found to be relatively unchanged from the room temperature values for thermal treatments up to 600°C. However, when the γ-alumina membrane was subjected to temperatures higher than 600°C, the permeance was found to change continuously at constant temperature. This was probably due to a gradual phase transformation of the material, as γ-alumina is known to undergo phase changes at these higher temperatures. Since the temperature required for methane coupling reactions is in excess of 750°C, γ-alumina may not be the ideal candidate since a leveling off of permeance is not realized.

Zirconia Membranes :

Zirconia membranes are stable at high temperatures, and are also available in pore sizes of less than 2000 Angstroms, but zirconia itself is a low level methane conversion catalyst allowing methane conversion to CO_x products. Studies in the literature have shown that though the zirconium-containing complex oxides catalyze the methane oxidative coupling reaction, they are not very active catalysts. Of all the zirconium containing catalysts, zirconia itself is the least effective. Khan and Ruckenstein [3] reported methane conversion of 2.4% , with a C_2 yield of 0.43% and C_2 and CO_x selectivity of 18% and 82% respectively at 750°C and CH_4/O ratio of 4.

Perovskite depositions on 1000 Angstrom zirconia membranes gave results similar to the ones in the α-alumina experiments. Complete pore closure was not achieved, though a drop in permeance of gases through the membrane was observed. A comparison with different pore size zirconia membranes, and the 2000 Angstrom alpha alumina membrane is made in Figure 9, showing the permeance of nitrogen gas through these different membranes that have been subjected to three perovskite (0.6M) depositions and treated at 200°C. Even though alpha alumina has a bigger pore size (2000 Angstrom), at the completion of the three depositions and thermal treatment, the permeance value in this alpha alumina membrane is comparable to the smaller pore size zirconia membranes, possibly indicating better wettability of alumina than zirconia.

Porous VYCOR Glass Membranes :

A possible alternative as a membrane material is porous VYCOR® (glass) membrane. Porous VYCOR® (commercial name "thirsty glass") is the intermediate porous leached form of the basic consolidated (non-porous) VYCOR. Corning Inc. markets this porous VYCOR® with

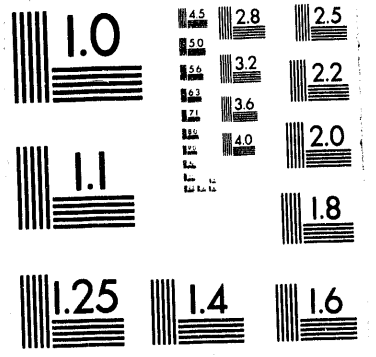
1.0
1.1
1.25
1.4
1.6
1.8
2.0
2.2
2.5
2.8
3.2
3.6
4.0
4.5
5.0
5.6
6.3
7.1
8.0
9.0

3 of 8

literature to select good methane coupling catalysts in general. Depending on what reactor configuration would be studied, synthesis of one of the selected catalysts would be undertaken.

Methane coupling catalysts can be classified under five broad categories. The first is (promoted) Group IIA Metal-Oxide catalysts. The most commonly used catalyst in this class is the Li/MgO catalyst which is an active catalyst but the C_2 yields are generally low [8,11]. La/MgO catalysts seem to exhibit higher yields and relatively higher selectivity for C_2 production. They are also superior to Li/MgO catalysts in that Lithium tends to evaporate and the catalyst loses its activity fairly rapidly at high temperatures of operation needed for methane coupling reaction. The second class of catalysts is the Lanthanide Metal-Oxide catalysts [9]. Oxides of La, Sm, Ce, promoted sometimes with alkali metals are the chief members of this class. The third category is the Transition Metal-Oxide Catalysts. Chlorides and oxides of alkali earth metals, which when used to promote members of this class, i.e., oxides of transition metals like Ti, Zn, Co, and Ni provide high C_2 yields in methane coupling reactions [5]. Significant literature is also present on the fourth class of catalysts namely the Group IIIA, IVA, and VA Metal-Oxide catalysts, though relatively low conversions and C_2 yields are obtained [10]. The last class of methane coupling catalyst are the Complex Oxide Catalysts, and the Perovskites (La-Sr-Fe-Oxides) come under this class [4,6,7].

A criterion that is normally employed to choose a catalyst is the yield of the favorable product that is produced by that catalyst. In this study, the reported literature C_2 yields were ratioed to a " theoretical maximum C_2 yield" to give a number that would be used as an index of the efficiency of the catalyst. This additional criterion, the 'theoretical maximum', is obtained by imposing limitations on the operating conditions and on what products are allowed to be formed. Thus for each of the reported catalysts, this criterion was employed to assess what would be the maximum theoretical C_2 yield of that catalyst.

The primary products observed in the high temperature oxidative coupling of methane are CO_2, H_2, C_2H_4, C_2H_6, CO_2, CO and H_20. If we assume that there are no CO_x products formed, then we can define a "maximum theoretical C_2 yield". Also, since most methane coupling reactions are carried out at low oxygen concentrations, we assume that there is no oxygen left in the end products to simplify the calculations. By incorporating the Gibbs Free Energy of formation of each species and its dependence on temperature, the conversion of the reactant species is computed to obtain yields of C_2 products, C_2H_4 and C_2H_6 . By summing the yields of both these C_2 products, a value for theoretical maximum C_2 yield is obtained. The catalysts listed in the table below are chosen based on this criterion. In addition to this criterion, traditional requirements on activity, selectivity, operating temperature, and longevity of the

catalyst, and the particular reaction configuration etc., have to be all considered in selecting a catalyst.

Table 4. Catalysts selected from literature based on theoretical maximum yield.

Catalysts	Authors	Temperature	CH_4/O_2 Ratio	Selectivity	C_2 Yield (Y)	Y/Y* (%)
$SrCe_{0.9}Yb_{0.7}O_{2.95}$	Machida [4](1987)	750°C	2	60.1%	31.6%	31.6%
$MnO/NaCl/TiO_2$	Feng-Chang [5](1989)	750°C	2.75	61%	26%	35.3%
$Pb_2Mn_2Si_2O_9/SiO_2$	Thomas [6] (1988)	800°C	7.7	67.5%	20.3%	67.2%
Li NiO_2	Kikhtyanin [7] (1987)	697°C	6	46.7%	12.1%	68.3%
Li/MgO	Lunsford [11] (1985)	720°C	2	50.3%	19.0%	19%

Modeling Results

To model the specific membrane reactor configurations and the kinetics of oxidative coupling of methane in these membrane reactors, certain simplifying assumptions were made in developing the computer model. Methane gas (diluted 50% in a helium stream) flows on the tube side and oxygen (or air), diluted with helium (1:4), flows on the shell side (tube and shell side total flow rates are set at 1ml/min). The catalyst is present only on the tube side(tube I.D. = 6.7 mm and O.D. = 10.24 mm.) and chemical reactions occur only on the tube side. Isothermal operation is assumed and calculations are carried out at a constant temperature of 800°C. Steady state operation is assumed, at isobaric conditions (i.e., no pressure gradient between shell and tube side). Depending on the pore size, Knudsen (pore size in the range of 50 Angstroms) or molecular diffusion is the transport mechanism considered. For porous catalytic membrane reactors, all the catalyst is assumed to be inside the pore structure and the flow rates on tube and shell sides are balanced so that there is no free oxygen seeping into the tube side. For dense membrane reactors, only oxygen gas is assumed to transfer from shell to tube side, and the value of permeability of the dense membrane to oxygen gas was adjusted to control a steady, low, flux of oxygen into the tube side. The kinetic rate expressions for the oxidative coupling reaction have been taken from Tung and Lobban [12], making adjustments for different reactor configurations as discussed below.

To compare the membrane reactors with conventional packed bed reactor, the geometry of the reactor was modified so that the well-mixed reactant gases (methane and oxygen) flow

only in the tube side which holds the packed bed. Since there is oxygen present in large quantities in a conventional packed bed reactor, gas phase kinetics have to be considered in modeling such a reactor. We have included this effect by modifying the kinetic rate expression (setting the coefficient of the CO_x production reaction to 1.35 in this and other configurations, as suggested by Tung and Lobban [12]). The kinetic constants are however left unchanged because of the lack of a better alternative. Though this does not present a completely realistic picture of gas phase reactions in a packed bed reactor, it will serve to present the differences in reactor performance between conventional and porous membrane reactors.

Figure 12 shows the modeling results of a packed bed reactor. The catalyst is packed in the tube and the tube side flow consists of a mixture of methane and oxygen in the ratio 3:1. The maximum C_2 yield is about 20% and is obtained at a reactor length of 0.1 m. All the oxygen is exhausted within this reactor length. The excess of oxygen availability at the reactor entrance allows CO_x formation reactions to occur at a competitive rate and C_2 selectivity is low at the reactor entrance. As more and more oxygen is consumed, the CO_x reactions are inhibited and selectivity increases. Because of availability of oxygen, methane conversion rises steeply and saturates at a value of 40% when there is no more oxygen for the reaction to proceed.

Figure 13 shows the simulation results for a porous membrane reactor with a pore size of 40 Angstroms and for a 4 Angstrom porous membrane reactor. At the entrance of the reactor, in the tube side (where the catalyst is present), selectivity is high at first, as there is initially a high methane-to-oxygen ratio. As the oxygen permeates into the tube, selectivity drops. As oxygen gets depleted, methane conversion also decreases and both selectivity and conversion (and hence the yield) remain constant when all the oxygen is exhausted. Since the reaction scheme used for modeling does not involve any reactions accounting for disappearance of C_2 products once formed, the C_2 yield curves stay horizontal. In the case of the 4 Angstroms porous membrane, the trough (minimum) in selectivity is spread out further down the reactor length and the absolute values of selectivity is higher, since now the oxygen transfer is slower than in the 40 Angstrom membrane. This slower oxygen transfer also causes a more gradual rise in the methane conversion curve and the maximum C_2 yield is about 35%, obtained at a reactor length of 0.15 m.

Figure 14 shows the results for a dense membrane reactor. The C_2 yields are highest in this reactor configuration. Here, oxygen permeability is varied to assess the reactor performance. For a value of $1.0X10^{-9}$ for oxygen permeability, a C_2 yield of 35% is obtained at a reactor length of 0.1 m (which is comparable with the earlier two configurations). When the permeability value is dropped to $1.0X10^{-10}$ mol/s.m^2.Pa., higher yields are obtainable because

of the high values of selectivity in this reactor configuration. However, since supply of oxygen is slow, methane conversion rises slowly and a longer reactor length (0.5 m) is needed.

Conclusions

- Though permeance has been lowered by depositing oxygen transferring perovskite in the porous α-alumina and zirconia membranes, pore closure has not yet been achieved.

- Gamma alumina membranes undergo structural changes and do not exhibit steady permeation rate for gases at temperatures above 600°C.

- Porous VYCOR shows stability of permeance to gas flows across the membrane at 750°C up to 96 hours and hence will be used as one of the membrane materials in the membrane reactors.

- A three-region VYCOR membrane has been fabricated, with porous central region and non-porous end regions.

- Catalyst selection is based on comparison of C_2 yields reported in the literature with theoretical maximum yields and also on special requirements specific to the reactor configuration.

- Preliminary results from kinetic modeling of membrane reactors show better C_2 yields with membrane reactors when compared to conventional packed bed reactors operating under approximately same conditions.

Future Work

New methods will be attempted to achieve complete pore blockage of porous membranes. Attempts will be made to understand the reasons for incomplete pore blockage in alumina membranes through SEM studies of membranes subjected to several depositions of the perovskite. Perovskite depositions will also be tried on porous VYCOR membranes. Techniques such as gas phase deposition may be attempted to enable production of dense membrane reactors which are selective only for oxygen permeation.

With the porous VYCOR membranes now fabricated, kinetic experiments will next be attempted. The first membrane reactor configuration that will be studied is the fixed bed porous membrane reactor. A suitable catalyst would also be chosen from the list of selected catalysts so that the porous membrane can be doped by depositing the catalyst or its pre-cursor from a solution of the catalyst and synthesize a catalytic porous membrane. A conventional packed bed reactor will also be studied. Comparison of C_2 yields and selectivities will then be made between a conventional packed bed reactor, a porous membrane packed bed reactor and a catalytic membrane reactor.

Future experiments with VYCOR membranes would also involve doping the membrane with various catalysts. Silica, which is the base material for VYCOR is not as receptive to metal oxide adhesion as is alumina and the amount of catalyst that can be loaded onto the membranes will be investigated. Analytical characterization of the porous VYCOR membranes using SEM will also be undertaken. Here too, VYCOR may pose problems in terms of sample preparation, in that glass tends to collect charge easily and build up static fields under electron beams if suitable electrical grounding of the sample specimen is not achieved. The membrane samples can be made more conductive through gold-palladium sputtering. Analytical studies will focus on obtaining the images of the porous structure of VYCOR and the distribution of perovskite in this porous structure (for VYCOR with perovskite deposits) by elemental mapping.

The modeling program will be modified to reflect a porous VYCOR membrane and reactions and transport inside the membrane pores. Comparison will be made between model predictions and experimental results from the catalytic membrane reactor. Experimental results from packed bed studies will also be compared with packed bed reactor model predictions, which will be improved to include gas phase reaction kinetics.

REFERENCES

1. Y. Teraoka, H.M. Zhang and K. Okamoto, N. Yamazoe, *Mat. Res. Bull.* 23, 51-58 (1988).

2. M.C. Kim, S.J. Park, H. Haneda, J. Tanaka and S.Shirasaki, *Solid State Ionics,* 239-243 (1990).

3. A. Z. Khan, E. Ruckenstein, *J. Catal.*, 139,(1), 304-21,(1992).

3. A. Z. Khan, E. Ruckenstein, *J. Catal.*, 139,(1), 304-21,(1992).

4. K. I. Machida, and M. Enyo, *J. Chem. Soc., Chem. Commun.* 1639 (1987).

5. W. Feng-Chang, Z.L. Chang, C.T. Au, and K.R.Tsai, Paper 26, presented at the *Symposium of Methane Activation, Conversion and Utilization*, Honolulu (1989).

6. J. M. Thomas, Xian Kuan, and Jaroslaw Stachurski, *J. Chem. Soc., Chem. Commun.* 162 (1988).

7. O.V. Kikhtyanin, V.M. Mastikhin and K.G. Ione, *Appl. Catal.*, 42 L1-L4, (1988).

8. Hongfu Shen, Xinping Wang, Qin Liu, Jing Shi, *J. Nat. Gas. Chem.* 1(2), 122-128 (1992).

9. K. Otsuka, Q. Liu, M. Hatano and A. Morikawa, *Chem. Lett.*,1835 (1987).

10. S. Ahmed and J.B. Moffat, Catal. Lett.,2:309 (1989).

11. T. Ito, J.X. Wang, C.H. Lin, and J.H. Lunsford, *J. Am. Chem. Soc.*, 107: 5062, (1985).

12. Wen-Yuan Tung and Lance L. Lobban, *Ind. Eng. Chem. Res.*, 31, 1621 - 1625 (1992).